Version of Record: https://www.sciencedirect.com/science/article/pii/S0958946522001305
Manuscript_432052c73d8ad07b12a3d082d445f25c

Multi-scale strategy to estimate the mechanical and diffusive properties of cementitious materials prepared with CEM II/C-M

Yushan Gu[a], Benoît Bary[a,*], Alisa Machner[b,c], Klaartje De Weerdt[b], Gerd Bolte[d], Mohsen Ben Haha[d]

[a] *Université Paris-Saclay, CEA, Service d'Etude du Comportement des Radionucléides, 91191, Gif-sur-Yvette, France*

[b] *Norwegian University of Science and Technology (NTNU), Department of Structural Engineering, Richard Birkelandsvei 1a, 7491, Trondheim, Norway*

[c] *Technical University Munich, Center for Building Materials, Professorship for Mineral Construction Materials, Franz-Langinger-Str. 10, 81245 Munich, Germany (Present address)*

[d] *Global R&D, HeidelbergCement AG, Oberklamweg 2-4, 69181, Leimen, Germany*

Abstract

A procedure to estimate the mechanical and diffusive properties of cement pastes, mortars and concretes made with a novel CEM II/C-M (S-LL) binder that has been developed within the European EnDurCrete project, is presented in this paper. The objective is to set up a strategy able to determine the materials composition at different scales and in various configurations, and to provide reliable estimates of the properties. The phase assemblages of the cement pastes upon hydration, and further exposed to carbonation, leaching with water or chloride containing solutions, are first simulated using thermodynamic modeling. Different homogenization schemes are then applied, to estimate the mechanical and diffusive properties of the hydrated and degraded materials at different scales. The interfacial transition zone (ITZ) in mortar and concrete is accounted for by means of specific hypotheses regarding its thickness and the respective volume fraction of hydrates and capillary pores. The application of the differential scheme (DIF) at the cement paste scale, and

*Corresponding author
Email addresses: yushanjoanna@hotmail.com (Yushan Gu), benoit.bary@cea.fr (Benoît Bary), alisa.machner@tum.de (Alisa Machner), klaartje.d.weerdt@ntnu.no (Klaartje De Weerdt), gerd.bolte@heidelbergcement.com (Gerd Bolte), mohsen.ben.haha@heidelbergcement.com (Mohsen Ben Haha)

at higher scales of the generalized self-consistent scheme (GSCS) or a procedure accounting for ITZ modeled as an interface combined with the DIF scheme, show a good consistency with the measured Young's modulus. In parallel, simulations are performed on 3D specimens composed of spherical particles surrounded by an ITZ layer to provide additional data for comparison. Numerical results and analytical estimations are found to be in excellent agreement. Finally, a specific study focusing on the effects of the ITZ on both mechanical and diffusive properties shows a significant impact of its thickness and its composition.

Keywords: Novel cementitious material, Thermodynamic modeling, Multi-scale modeling, Mechanical and diffusive properties, 3D computational analysis, Interfacial transition zone (ITZ).

---

1. Introduction

A novel CEM II/C-M (S-LL) binder, which consists of 50 wt.% Portland cement clinker, 40 wt.% granulated blast-furnace slag and 10 wt.% limestone, has been designed within the European Horizon 2020 project EnDurCrete. Cementitious materials prepared with this binder have shown a good resistance to carbonation [1] and a high potential for long-term sustainability. As is well-known, elastic and diffusive parameters are of uttermost importance to quantify the mechanical behaviour and transport properties of concretes, which are in turn essential to characterize the durability and predict the service-life of reinforced concrete structures.

The estimation of the property of composite materials has been extensively investigated in the literature, e.g. [2, 3] among others. To estimate the mechanical and diffusive properties of cementitious materials, analytical upscaling methods have proven to be very efficient. Such methods have been applied in many situations to estimate various properties as elastic (see e.g. [4, 5, 6]), viscoelastic (e.g. [7, 8]), strength (e.g. [9, 10]), diffusivity (e.g. [11, 12, 13]) to cite a few. They rely on an appropriate representation of the microstructure of the material in terms of volume fraction and morphology of the elementary phases, associated with an accurate characterization of their properties. To obtain these data may be challenging when the microstructure evolves, e.g. due to hydration or chemical degradation. In many studies, simplified and/or empirical models have been applied to describe such microstructure evolution, leading generally to relatively satisfying results in particular in the case of hydration, see e.g. [12, 14]. However, when dealing with new

materials for which little data is available, and also to increase the understanding and accuracy of phase assemblage changes when investigating various exposure situations, much more advanced tools must be deployed. The most versatile strategies have to account for complex chemical reactions occurring between all considered phases and the species present in the pore solution, to determine the progressive evolution of phases with time. In this respect, the Gibbs free energy minimization software GEM-Selektor (GEMS) has been widely applied in the literature [15, 16, 17, 18] to simulate the thermodynamic changes in the phase assemblage of cementitious materials upon different conditions, e.g., hydration, carbonation, and exposure to solutions containing aggressive substances. The advantages of employing GEMS to simulate the phase equilibrium in a fluid-solid system are reflected in the relevance of chemical description, robustness of results, mass balance accuracy, numerical stability, high speed, and portability to high-performance computing systems [18]. With the phase assemblages simulated by GEMS, both microstructure and composition of the materials can be precisely modeled.

Cementitious materials are generally considered as heterogeneous materials at several levels: at micro-scale for cement paste, at meso-scale for mortar and at macro-scale for concrete. To apply upscaling procedures to estimate physical properties, a proper representation of their microstructure has to be chosen. Various descriptions have been proposed in the literature, from very simple ones based on spherical inclusions embedded in a homogeneous matrix, to more sophisticated ones including non-spherical shapes for the inclusive phases, the latter being not necessarily homogeneous. Besides, the interfacial transition zone (ITZ) has an important effect on both mechanical and diffusive properties of mortar and concrete [19, 20], due to its higher porosity compared to that of bulk cement paste [21]. Few studies have managed accurately measuring the properties of the ITZ, due to its small size compared to aggregates, and the fact that the ITZ is not a homogeneous interface but rather a graded phase [22]. The characteristics of the ITZ have been estimated by inverse analyses from macroscopic experimental values on mortars, considering a simplified homogeneous ITZ, in several studies, see e.g. [23, 24]. However, non-consistent results have been found upon these studies [25]. Alternatively, upscaling techniques have been used in e.g. [26], based on convenient hypotheses regarding the ITZ composition with respect to the plain hardened cement paste (HCP) one. This approach is associated with a representation of HCP microstructures by a doubly coated spheres assemblage model (see also [27]), where the remaining anhydrous phase is

the core surrounded by the inner and outer coatings representing respectively high-density and low density C-S-H layers, both embedding inclusions of all other mineral phases and pores.

It is important to recognize that without the precise knowledge of the volume fraction of the phases and their morphology (i.e. spatial arrangement, shapes of inclusions etc.) at different scales, upscaling techniques cannot in general be applied successfully and confidently. Moreover, these characteristics allow the selection of the most appropriate homogenization procedure. Various approximation schemes have been proposed and used in the literature to estimate the mechanical and diffusive properties of cementitious materials. For example, the self-consistent scheme (SC) [28, 29], adapted for disordered materials, is capable to predict a percolation threshold that is useful for mimicking the setting at early ages. On the other hand, the Mori-Tanaka scheme (MT) [30] and the differential scheme (DIF) [31] well illustrate a composite material made of inclusions distributed in a known matrix phase. The DIF scheme is a less commonly adopted approximation scheme in cementitious materials and is based on the idea of incremental homogenization, i.e. the inclusions are added by small quantities so that the dilute scheme can be applied at each step. The generalized self-consistent scheme (GSCS) [32], and the replacement procedure [33] combined with one of the SC, MT and DIF schemes, are able to estimate the properties of mortar and concrete, taking into account the existence of the ITZ around the sand or aggregate particles. However, these various schemes and methodologies give in general different estimations, and comparison/validation data are required to determine the best suited homogenisation scheme for the considered case. In this respect, experimental measurements provide the most direct data to be compared with the analytical estimations; 3D computational analysis represents another way. One advantage of the numerical procedure is that it can afford very complex microstructures, the main limitation being the size of the problem to solve. It has been used e.g. to study the effect of aggregate shapes on mechanical behaviour and diffusivity of mortars [34], the creep behaviour of concrete [35], the initiation and propagation of cracks [36, 37], and constitutes an alternative way to predict the properties of materials and to further support the choice of the most appropriate homogenization scheme.

In this paper, we present a procedure to estimate the mechanical and diffusive properties of saturated cement pastes, mortars and concretes prepared with a novel CEM II/C-M (S-LL) binder. It is worthy to mention that our main objective is to propose a strategy based on the combination of

different complementary tools that may be extended to other materials, rather than new upscaling schemes or microstructure descriptions. After having defined the studied materials, the procedure starts from the phase assemblage simulation of cement paste by the software GEMS, for determining the cement paste composition upon various conditions. Then the mechanical and diffusive properties of the hydrating materials at different scales are estimated from cement paste to mortar, and subsequently extended to concrete, based on simple microstructure representations and the application of different homogenization schemes. As an important phase in mortar and concrete, the ITZ is assumed to be composed of hydrates and capillary pores from the cement paste, with additional pores for the remaining space. The best suited homogenization schemes are determined by comparing the obtained estimations to the experimental measurements of Young's modulus. Moreover, a 3D computational analysis is performed to further confirm the validity of the adopted homogenization schemes. In particular, simulation data are provided with specimens exhibiting spherical particles surrounded explicitly by a ITZ layer. The effects of the ITZ thickness and its composition on the properties of mortar are further investigated, and the estimated properties of the ITZ in mortar and concrete fabricated with the novel binder are provided thereby. In the last part of the paper, the procedure is applied to estimate the mechanical and diffusive properties of materials exposed to carbonation, leaching with water and chloride containing solutions.

2. Materials with novel binders

In this section, the materials made with the CEM II/C-M (S-LL) binder considered in this study with water to cement (w/c) ratios of 0.40, 0.45, 0.50 and 0.60, are described. The cement constitutive properties and data on hydration products and microstructure description are provided in [38]. All materials are exposed to hydration, then the materials with w/c=0.60 are further exposed to carbonation after 76 days of hydration, and the materials with w/c=0.45 are exposed to leaching with water and chloride containing solutions (NaCl/NaCl+KOH) after 146 days of hydration. Table 1 shows the mix designs of mortar and concrete samples in terms of volume fractions of different components, which are important input to estimate the mechanical and diffusive properties of cementitious materials. The w/c ratio given in Table 1 represents the effective water content, which means that the water content of the aggregates and the adsorption of water on the aggregates in the

Table 1: Mix design of materials exposed to hydration, carbonation, leaching with water and chloride containing solutions.

Dosages (L/m^3)	C. 0.45	M. 0.45	C. 0.50	M. 0.50	C. 0.60	M. 0.60
CEM II/C-M (S-LL)	105	188	117	184	105	163
Washed sand 0/4	350	546	343	542	357	551
Washed gravel 5/10	140	-	111	-	79.7	-
Washed gravel 10/15	210	-	247	-	264.6	-
VC-2014 (SP)	1.79	1.79	1.22	1.22	0.4	0.6
VF-10150666 (polif)	2.8	2.6	1.92	1.83	0.7	0.9
Water	189	241	175	264	189	292
Exposed conditions	Hydration Leaching Chloride ingress		Hydration - -		Hydration Carbonation -	

* C. stands for concrete samples, and M. stands for mortar samples.

* The average diameters for aggregates washed sand 0/4, washed gravel 5/10, and washed gravel 10/15 are 1.50 mm, 7.98 mm, and 10.57 mm.

* The water absorption of aggregates washed sand 0/4, washed gravel 5/10, and washed gravel 10/15 has been measured as: 1.3%, 0.9%, and 0.7%.

fresh state have been taken into account. The fine aggregate used in mortar is a washed sand 0/4 with an average diameter of 1.50 mm, and the two coarse aggregate types adopted in concrete samples are washed gravel 5/10 and washed gravel 10/15, which have an average diameter of 7.98 mm and 10.57 mm, respectively. The dimensions of aggregates are important, to determine the volume of the ITZ, as will be explained in detail in section 3.2.2. Mortar prisms ($40 \times 40 \times 160$ mm) cast with CEM II/C-M (S-LL), sand and a w/c of 0.40, 0.50 or 0.60, are fabricated within the project to measure their Young's modulus; the obtained values will be compared with the simulations. The mix design of the mortars is shown in Table 2.

Table 2: Mix design of the mortars used to measure the Young's modulus that are to be compared with the estimations.

w/c	Cement (kg/m^3)	Sand (kg/m^3)	Water (kg/m^3)
0.40	511.2	1350.0	204.5
0.50	450.0	1350.0	225.0
0.60	401.9	1350.0	241.1

3. Phase assemblages and estimation procedures

3.1. Phase assemblages from GEMS

As mentioned in the introduction, the Gibbs free energy minimization software GEM-Selektor v.3 (GEMS3) [15, 16, 17, 18] is applied to simulate the thermodynamic changes in the phase assemblage of the cement paste when it is exposed to hydration and degradation conditions, with the thermodynamic data taken from the PSI-GEMS database and a cement-specific database (CEMDATA 18) [39]. Chemical reactions are assumed to be in thermodynamic equilibrium in a closed system, i.e. with no transport considered. As this is not the main focus of this paper, we give in this subsection only a brief description of the results obtained; a much more detailed interpretation of the phase assemblages will be provided in a dedicated contribution. The hydration of the novel binder calculated by thermodynamic modeling is based on the experimental data concerning the reaction degree of phases. The reaction degree of cement components was quantified by PONKCS analysis of X-ray powder diffraction (XRD) scans on hydration stopped cement paste at discrete hydration time intervals, and the reaction degree of the various supplementary cementitious materials (SCMs) was determined by scanning electron microscopy (SEM) coupled with energy dispersive spectrometry (EDS), see [38]. The data was used as input for the thermodynamic modeling, and the results of thermodynamic calculations were observed to be qualitatively in accordance with the experimental data.

Fig. 1 shows the modeled phase assemblages expressed in volume [cm^3] for 100 g of the hydrating CEM II/C-M (S-LL) binder as a function of the time, for the w/c ratios of (a) 0.45, (b) 0.50, and (c) 0.60 at 20 °C. The precipitated hydration phases are C-S-H, portlandite (CH), ettringite, monocarbonate, hydrotalcite, and siliceous hydrogarnet. By plotting the results in [cm^3/100 g],

the (theoretical) chemical shrinkage due to the volume change of free and bound water is visible as well.

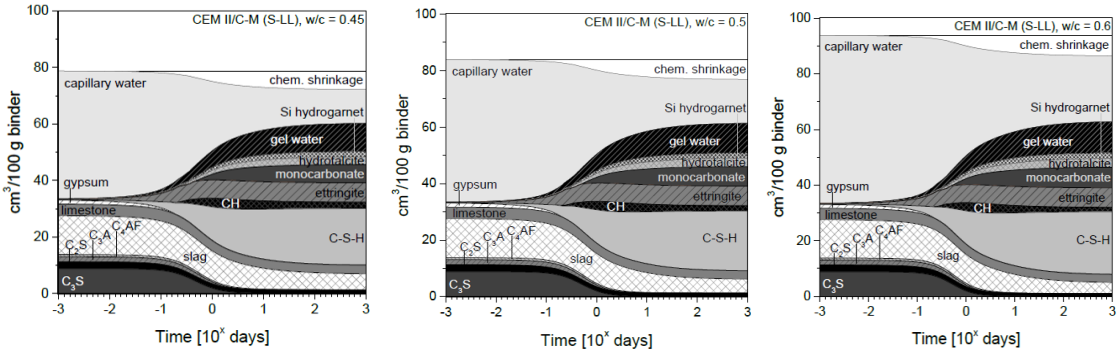

(a) w/c= 0.45; (b) w/c= 0.50; (c) w/c= 0.60.

Figure 1: Modeled phase assemblage plotted as a function of time for the hydrating CEM II/C-M (S-LL) binder with w/c ratios of (a) 0.45, (b) 0.50, and (c) 0.60 at 20 °C.

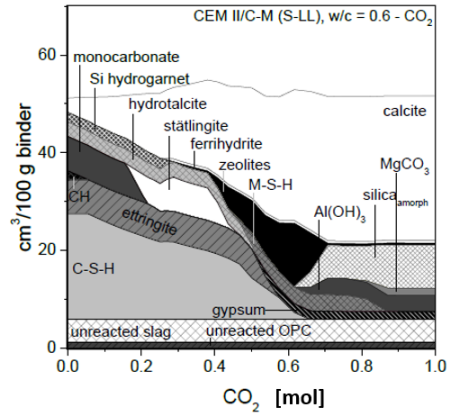

Figure 2: Modeled phase assemblage plotted in [cm^3/100 g] as a function of added CO_2 [mol] for the 76 days hydrated CEM II/C-M (S-LL) binder with a w/c ratio of 0.60 at 20 °C.

Fig. 2 shows the calculated phase assemblage of the CEM II/C-M (S-LL) binder prepared with a w/c ratio of 0.60 and hydrated at 20 °C for 76 days in [cm^3/100 g], and subsequently exposed to an increasing amount of CO_2 at 20 °C. With this progressive addition of CO_2, the hydration phases decompose and react to form calcite and various other residual phases, such as gypsum, $Al(OH)_3$, $MgCO_3$, amorphous silica, zeolites and ferrihydrite. Strätlingite and M-S-H are appearing as transition phases between the initial phases and the residual phases at the highest amount of

CO_2 added. Note that thermodynamic modeling has been a popular method to investigate the phase assemblage of cementitious materials exposed to carbonation, e.g. [40, 41, 42] among others, and the calculations have been proved to agree well with the experimental data. For instance, such calculations have shown a good consistency with the data from TGA and XRD [42], and the calculated total porosity has been found to be close to the value measured by MIP [43].

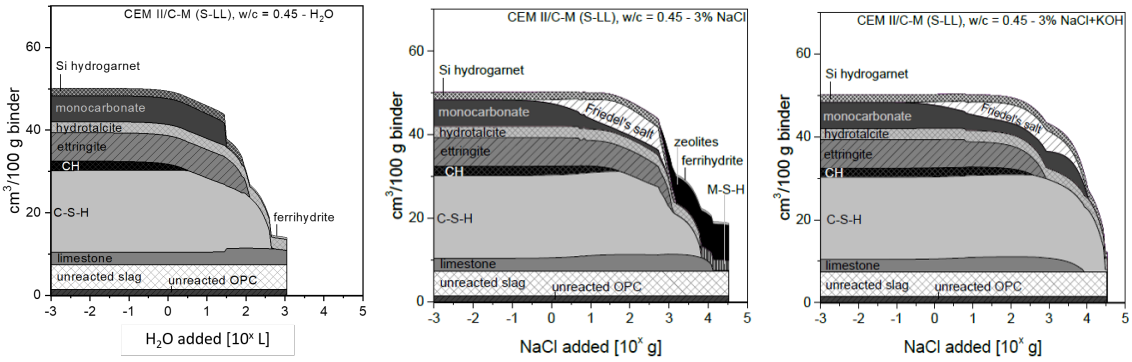

(a) H_2O; (b) 3% NaCl solution; (c) 3% NaCl+KOH solution.

Figure 3: Modeled phase assemblage plotted in [cm^3/100 g] as a function of added H_2O [10^x L] (a) or NaCl (b)-(c) [10^x g] for the 146 days hydrated CEM II/C-M (S-LL)-0.45 binder at 20 °C, exposed to either (a) H_2O, (b) a 3% NaCl, and (c) a 3% NaCl+KOH solution.

Fig. 3 shows the simulated phase assemblage of the CEM II/C-M (S-LL)-0.45 binder hydrated for 146 days at 20 °C, and subsequently exposed at 20 °C either to leaching with water, a 3% NaCl solution or a 3% NaCl+KOH solution, as a function of the volume of added solution (a) or the mass of NaCl (b)-(c). It should be pointed out that the estimations of thermodynamic modeling in such cases have been proven to be consistent with the experimental data. For instance, authors in [42] have compared the phase assemblage of cement-based materials exposed to leaching calculated by thermodynamic modeling with the results experimentally measured using TGA and XRD, and the results have shown good consistency regarding the complete decomposition of portlandite, the presence of hydrotalcite, etc. Moreover, the experimental observations concerning the transformation of monocarbonate to Friedel's salt and calcite, and the leaching out of Friedel's salt, portlandite, and C-S-H at the exposed surface have also been confirmed by thermodynamic modeling [44]. The phases present at the start of the modeling are equal to the phases calculated by the hydration model at 146 days. As expected, the results upon H_2O exposure mimicking leaching show a progressive

dissolution of the initial phases. By plotting the results obtained with the addition of NaCl (Fig. 3(b)), we observe that monocarbonate transforms into Friedel's salt. During this transformation, chloride ions replace carbonate ions in the interlayer of the AFm phase; therefore, slightly more limestone (calcite) is predicted to form. Note that in this modeling, the exposure to NaCl is coupled with the exposure to leaching with water. Such high amounts of NaCl solution lead to a combined leaching attack on the hydrated cement. Therefore, the hydration phases start to decompose at a certain amount of chloride solution added and transform into less soluble residual phases such as M-S-H, zeolites and ferrihydrite. In the last studied case of degradation (Fig. 3 (c)), a small amount of KOH is added in the exposure solution, with the aim to decrease its leaching effect by increasing the pH. To maintain a similar concentration of potassium in the NaCl+KOH exposure solution compared to the pore solution of hydrated cement paste after 146 days (approx. 150 mmol/L), 8.16 g KOH was added to 970 g H_2O before preparing the NaCl+KOH solution. We can indeed observe from the results that for the same quantities of solution added as for the 3% NaCl case, larger volumes of C-S-H, hydrotalcite and siliceous hydrogarnet remain stable, indicating a reduced dissolution process attributed to KOH.

3.2. Representation of materials and upscaling methods

The representative microstructures at the different scales considered and the adopted approximation schemes are presented in this section. As indicated in the introduction, here the objective is to develop a procedure to estimate the material properties based on a simplified representation of the microstructure at each scale, by using classical homogenization schemes. In cement paste, the phases of hydrated products, anhydrous phases, capillary water, and empty pores are considered, and three common approximation schemes, namely MT, SC, and DIF, are tested and compared. The second level, mortar, is represented by a 2-layer composite sphere assemblage model: the fine aggregate (sand) is the core of the sphere, and is surrounded by the ITZ, with the cement paste being the outer layer. The main assumptions concerning the ITZ will be explained in detail in section 3.2.2. At the level of concrete, a composite sphere assemblage model similar to the mortar microstructure but with the coarse aggregate as the core instead of the sand, is retained, with the external layer composed of the mortar homogenized at level II. Two approximation procedures are used to estimate the mechanical properties of materials exhibiting composite spheres: the GSCS

[32], and the so-called replacement procedure [33, 35], in which the ITZ is modeled as an interface, combined with one of the classical schemes among MT, SC, and DIF. Only the GSCS is applied for the estimations of diffusive properties. Note that as the respective formulations of these classical schemes are well-known, they will not be recalled here for the sake of brevity.

3.2.1. Cement paste

One important hypothesis at this scale is that C-S-H is considered as a composite phase comprising the solid C-S-H and gel pores filled by water, which means that the volume of C-S-H is the sum of these two phases that are determined separately in the GEMS simulations (see Fig. 1). The volume ratio of the solid C-S-H to the gel water is calculated to be approximately 2:1 in the GEMS simulations, with the assumption that C-S-H contains 2 mol H_2O per mol C-S-H as gel water. This assumption is based on the studies reporting that C-S-H contains approximately 4 mol H_2O per mol C-S-H in total including structural and gel water [45], and 1.5 – 2.2 mol H_2O per mol of Si as structural water when its Ca/Si ratio is between 0.8 and 1.45 [46], hence the average value of 2 mol H_2O. A ratio of Ca/Si in a range of 0.6 to 1.5 is used in the model of C-S-H in GEMS [47]. As mentioned, a one-level representative microstructure [4] is considered at this level as shown in Fig. 4: hydrates, anhydrous phases, and capillary water are introduced as spherical inclusions embedded in the matrix composed of the homogeneous C-S-H phase. The real shape of particles in cement paste is obviously more complicated (see e.g. [12, 26, 48]), and it has an effect on the volume fraction of the ITZ in mortar or concrete [49], and inevitably on the effective elastic modulus and diffusivity of composites [50, 51, 52]. However, the spherical particle approximation was found to provide satisfactory results especially when both the volume fraction of the inclusions and the contrast of properties between the matrix and the inclusions are low to moderate [53, 3, 54]. At the scale of cement paste, the effect of representing ettringite (needle-like) and portlandite (disk-like) by prolate and oblate spheroids was shown to be low [53], while the other phases have been kept spherical since few evidences indicate their geometry. In mortar and concrete, a slight influence of the aggregate shapes has been reported [35, 55, 56] mainly due to the limited contrast of mechanical properties between the matrix and inclusion phases.

The one-level microstructure combined with one of the three upscaling schemes: MT, SC, and DIF,

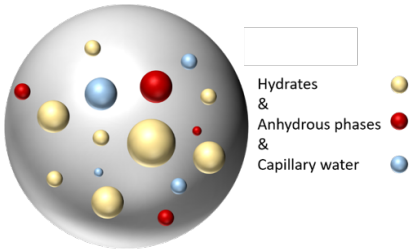

Figure 4: Simplified representative microstructure of cement paste in one level.

is used to estimate the mechanical and diffusive properties of cement paste. The scheme giving the most acceptable results will be subsequently retained for the final estimations. In the MT scheme, C-S-H is considered as the matrix, in which the spherical inclusions are distributed. In the SC scheme, all phases have the same status and are assumed to be included in an effective matrix whose properties are yet unknown; the effective properties are then the solution of implicit equations. In the DIF scheme, C-S-H is considered as the initial matrix, and the other phases are added progressively to the effective matrix through an iterative procedure. Here, we have chosen to add simultaneously all the inclusive phases. However, other choices can be made, for instance the phases may be added entirely one after the other. Such addition procedure has been found to have negligible effects on the estimations through several trials in our study, not shown here for conciseness. Concerning the diffusive properties of cement paste, C-S-H and capillary pores are considered diffusive, and the other phases are assumed to be perfectly insulating [27].

3.2.2. Mortar and concrete

As explained above, the classical choice for representing the microstructure of both mortar and concrete is based on an assemblage of composite spheres, as presented in Fig. 5. At the scale of mortar, the fine aggregate is the core of the composite sphere, and is surrounded by a first layer representing the ITZ and a second one the bulk paste. Note that the bulk paste in mortar is supposed to be composed of the same phases as the cement paste [26], but with very slightly different volume fractions due to the presence of the ITZ. This 2-layer composite sphere is subsequently embedded in the yet-unknown effective material of mortar. At the scale of concrete, mortar is in turn considered as the external layer of the double coated spheres, the coarse aggregate and the ITZ representing

their core and first layer, respectively. One advantage of this representation is that the GSCS [32] provides directly exact or very accurate estimations of diffusive and mechanical properties, see e.g. [14, 24]. The equations giving the expressions for Young's modulus, shear modulus, and diffusive coefficient of materials are well known and are recalled in Appendix A.

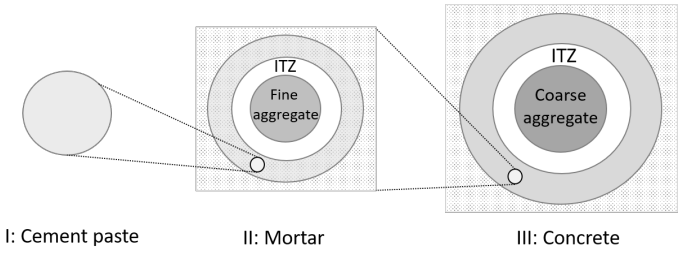

Figure 5: Representative microstructures of cementitious materials at different scales.

At the scales of mortar and concrete, the ITZ is assumed to have identical properties. Moreover, its thickness is supposed not to depend on particle size [57, 58], and values between 15 and 40 μm [23] are commonly adopted in the literature, with an average of about 20 μm [26, 59]. In this paper, an ITZ thickness of 16 μm has been shown to give satisfactory estimations and has been retained. To be more specific, the estimated Young's modulus and diffusive coefficients of mortar and concrete are consistent with the data reported in the literature and measured in our project, which will be explained in details in sections 4.1.2 and 4.4. We also make the hypothesis that the ITZ has an identical composition as the cement paste but with a higher porosity for the sake of simplicity, though the ITZ may have a higher volume fraction of calcium hydroxide and AFt, and a lower volume fraction of C-S-H compared to the bulk paste in mortar. Note that for the mechanical properties, a higher volume fraction of calcium hydroxide and AFt will increase the Young's modulus of the ITZ, while a lower volume fraction of C-S-H will decrease it. Since it is complicated to simulate the real composition of the ITZ without extra information, we have preferred to simplify the description. Besides, it should also be pointed out that ITZ percolation is not taken into account directly, although it may have some effects on the macroscopic properties. More sophisticated approaches may be used as e.g. [60, 61, 62] to address this aspect, which is out of the scope of this paper. Moreover, it is also worth mentioning that the percolation threshold concerning the porous network of materials, which depends on the distribution and the shape of inclusions [63], the ITZ thickness [64], etc., has not been considered directly in this work. This

aspect is addressed indirectly through the C-S-H phase that is assumed to be diffusive and always percolates. Some hydrates and capillary pores of cement paste, which have a volume fraction of α relatively to the total volume of cement paste, are then assumed to be transferred to the ITZ, and the remaining space of the ITZ is occupied by pores. With this assumption, a higher porosity in the ITZ than in bulk cement paste is obtained, as reported in e.g. [48]. This part of hydrates and capillary pores transferred to the ITZ is subtracted from the bulk paste in mortar. The effect of α on the properties of ITZ and mortar will be analyzed in section 4.4.

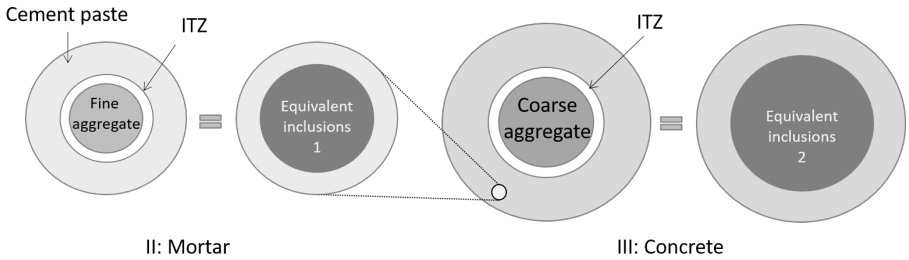

Figure 6: Replacement procedure for mortar and concrete.

An important specificity of the microstructure representation leading to the GSCS is that the whole space is filled with doubly coated spheres, with sizes going to the infinitesimal. Therefore, as the composite spheres are homothetic, the thickness of the ITZ varies for each sphere, contrary to the hypothesis mentioned above and supported experimentally. To circumvent this drawback and to test another approach to estimate the elastic parameters, an alternative homogenization method, termed as replacement procedure, is also applied. It consists in replacing aggregates and the ITZ by an energetically equivalent homogeneous spherical inclusion [33], see Fig 6. To be more specific, the fine aggregate and the surrounding ITZ are substituted by an equivalent phase, which is further embedded in the bulk paste to form mortar. Similarly, at the scale of concrete, a homogeneous particulate phase with properties equivalent to the ones of the coarse aggregate surrounded by the ITZ is distributed in the mortar phase. In this method, the ITZ is modeled as a thin interface whose thickness is much smaller than the aggregate size, and whose elastic properties are lower than the inclusion ones. In this case, the linear spring model [65] is well adapted to rule its behavior. Upon these conditions, the rigidity tensor of the interface can be expressed as:

$$\widetilde{\boldsymbol{k}} = \widetilde{k_n}\boldsymbol{n}\otimes\boldsymbol{n} + \widetilde{k_t}\boldsymbol{s}\otimes\boldsymbol{s} + \widetilde{k_t}\boldsymbol{t}\otimes\boldsymbol{t} \tag{1}$$

with $k_n = \frac{2\mu_{\mathrm{ITZ}}(1-v_{\mathrm{ITZ}})}{h(1-2v_{\mathrm{ITZ}})}$, $k_t = \frac{\mu_{\mathrm{ITZ}}}{h}$; $\boldsymbol{n}$ is the unit vector normal to the interface; $\boldsymbol{s}$ and $\boldsymbol{t}$ are the two orthogonal unit vectors in the tangent plane of the interface (see Fig. 7). Once the composite inclusions are replaced by the equivalent ones (whose mechanical properties are given in Appendix B), a classical homogenization method (MT, SC or DIF) can be applied to obtain the overall properties of the material. A summary of the approximation schemes that are adopted at the different scales is presented in Table 3.

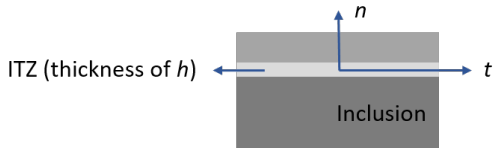

Figure 7: Schematic representation of a thin interface between an inclusion and a matrix.

Table 3: Summary of the approximation schemes applied at the different scales.

	Cement paste	Mortar	Concrete
Mechanical properties	MT	GSCS	GSCS
	SC		
	DIF	Replacement procedure	Replacement procedure
Diffusive properties	MT	GSCS	GSCS
	SC		
	DIF		

As already mentioned, the volume fractions of the considered phases are essential input for the property estimations of materials. While the GEMS simulations provide the volume fractions of hydrates, anhydrous phases, capillary pores and empty pores, the mix designs of mortar and concrete (Table 1) allow the determination of the volume fractions of the bulk paste and aggregates. Once the volume ratio of the ITZ : aggregates is determined based on the diameter of aggregates and the ITZ thickness, the volume fraction of the ITZ in mortar and concrete can be deduced. As noted in Table 1, the average diameters for aggregates washed sand 0/4, washed gravel 5/10, and washed sand 10/15 are 1.50 mm, 7.98 mm, and 10.57 mm, respectively, according to their particle size distributions. Consequently, the average diameter of the fine aggregate in mortar is 1.5 mm, and for the coarse aggregates in concrete it is deduced from:

$$D_{\text{coarse aggregate}} = 7.98\ \text{mm} \times \phi_{\text{coarse aggregate 1}} + 10.57\ \text{mm} \times \phi_{\text{coarse aggregate 2}} \tag{2}$$

where $\phi_{\text{coarse aggregate } i}$ is the volume fraction of the i-th coarse aggregate.

3.3. Properties of the elementary phases

The mechanical properties of each considered phase are taken from the literature, and for some phases, for which no mechanical properties are available, we used the properties of phases with a similar chemical composition. We assume that all pores predicted by thermodynamic modeling are accessible and well connected, which means that the inaccessible isolated pores are not considered. The pores saturated with water are assumed to have a bulk modulus of 2.2 GPa and a null shear modulus [66]. This information is summarized in Table 4. Regarding the diffusive properties, three phases are considered diffusive in the simulations: C-S-H, capillary pores, and the ITZ. The diffusion coefficient of C-S-H: $\mathrm{D_{C-S-H}} = 0.0025\ D_{\text{bulk water}}$ [67] is adopted, and $D_{\text{bulk water}} = 2.24 \times 10^{-9}$ $\mathrm{m^2/s}$ is taken from [34]. The assumptions concerning the ITZ have been explained in section 3.2.2 and their effects will be analyzed in detail in section 4.4.

Table 4: Summary of the phases considered in the material and their corresponding mechanical properties: Young's modulus (E) and shear modulus (μ).

Mineral name	E (GPa)	μ (GPa)	Ref.	Mineral name	E (GPa)	μ (GPa)	Ref.
C-S-H	22.4	9.0	[68]	Portlandite (CH)	42.3	16.3	[68]
Gypsum	45.7	17.2	[68]	Ettringite (AFt)	26.0	9.3	[69]
Monosulfate (AFm)	30.2	11.6	[69]	Monocarbonate	Same as AFm	Same as AFm	[68]
Hemicarbonate	30.2	11.6	[69]	Siliceous hydrogarnet	167.0	64.2	[70]
Hydrotalcite	30.2	11.6	[71]	Alite	135.0	51.9	[72]
Belite	130.0	50.0	[72]	Tricalcium aluminate	145.0	55.8	[72]
Ferrite	125.0	48.1	[72]	Slag	46.9	18.0	[73]
Calcite	76.0	29.2	[74]	Strätlingite	31.4	12.1	[69]
$CaCl_2$	Same as CH	Same as CH	[68]	Friedel's salt	Same as AFm	Same as AFm	-
$Al(OH)_3$	Same as CH	Same as CH	-	Silica amorph	72.8	31.2	[68]
Magnesite	Same as Limestones	Same as Limestones	-	Magnesium Silicate Hydrate	Same as C-S-H	Same as C-S-H	-
Ferrihydrate	Same as Silica amorph	Same as Silica amorph	[68]	Zeolites	Same as C-S-H	Same as C-S-H	-
Empty porosity	0.0025	0.001	[71]	Aggregates	70.0	26.9	[35]

4. Estimations of hydrating materials

In this section, the different schemes and procedures described in the previous sections are applied, to estimate the properties of cement paste, mortar, and concrete prepared with the novel CEM II/C-M (S-LL) binder, upon hydration. For conciseness, detailed results will be provided only for the case with w/c of 0.50. The denomination adopted for the different estimations are as follows: scheme (cement paste) + scheme (mortar) + scheme (concrete). For example, MT+MT+MT means that the MT scheme is used for the estimations of cement paste, then the replacement procedure associated with MT scheme is applied to estimate the (mechanical) properties of mortar and concrete. With the same definition, MT (cement paste) + GSCS (mortar) + GSCS (concrete) will be simplified as MT+GSCS+GSCS. In sections 4.1 and 4.2, we retained the ITZ thickness of 16 μm, and a 7.3 vol% (α) of hydrates and capillary pores in cement paste transferred to the ITZ, as explained in section 3.2.2.

4.1. Mechanical properties

4.1.1. Estimation results

Fig. 8(a) presents the estimated Young's modulus of cement paste with the CEM II/C-M (S-LL)-0.50 binder at 20 °C upon hydration via the MT, SC, and DIF schemes, as a function of time. A significant difference is observed among the results obtained by the different schemes at the early age of hydration. The MT scheme gives a Young's modulus above 10 GPa at the beginning of hydration, which makes no sense from a physical point of view. This is probably caused by the fact that at early ages the matrix, which is composed by the C-S-H phase in the case of MT scheme, has a very low volume fraction, meaning that the particulate phases fill (almost) all space. This configuration therefore largely exceeds the theoretical validity domain of the MT scheme, leading to unreasonable results. Unsatisfactory estimations of the mechanical properties at early-age by the MT scheme have also been reported in, among others, [75]. For this reason, the MT scheme associated with the proposed simple microstructure representation will not be considered at the cement paste scale. Compared to the results using the MT scheme, the estimations obtained by the DIF scheme are more acceptable. This can be explained by the fact that for each calculated point,

the matrix phase starts from C-S-H and is updated gradually with the addition of inclusions, leading to a significant decrease of the effective estimated properties compared to the estimation via the MT scheme. The Young's modulus of approximately 0 observed in the DIF estimation corresponds to a hydration degree of 0.01, calculated according to the phase assemblages from GEMS simulations. A percolation threshold of the SC scheme is observed when the hydration degree is around 0.19, which is close to the measurements between 0.17 and 0.25 for concrete with a w/c of 0.50 that have been reported in [76, 77].

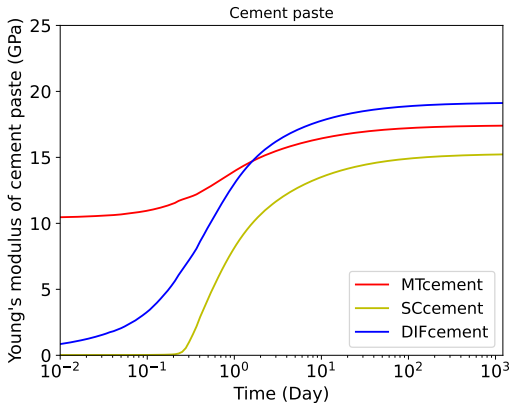

(a) Estimated Young's moduli of cement paste;

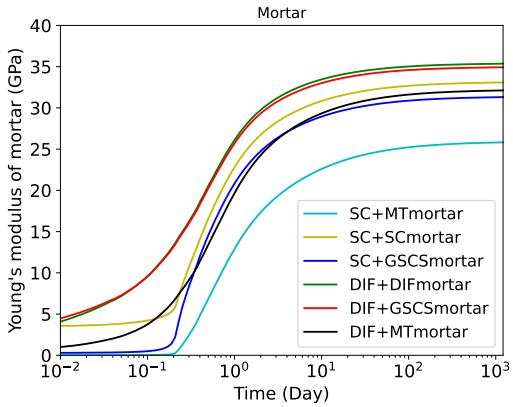

(b) Estimated Young's moduli of mortar;

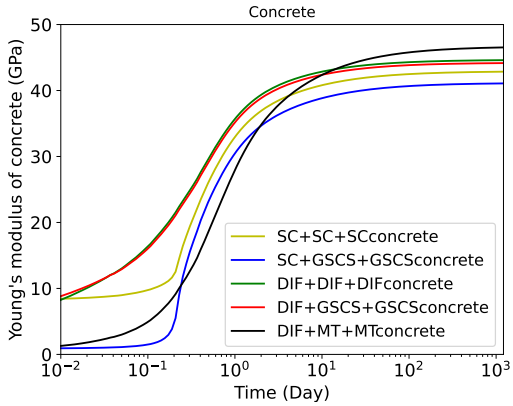

(c) Estimated Young's moduli of concrete.

Figure 8: Estimated Young's moduli upon hydration of (a) cement paste, (b) mortar, and (c) concrete with the CEM II/C-M (S-LL)-0.50 binder at 20 °C.

The Young's modulus evolution of mortar and concrete prepared with the CEM II/C-M (S-LL)-0.50 binder during hydration at 20 °C estimated with different schemes are presented in Fig. 8(b) and (c). The percolation threshold observed on the SC estimation of cement paste has disappeared when extending to mortar by the SC+SC scheme, due to a volume fraction of 53.1% for sand, which is higher than the 50% known to induce a percolation of the corresponding phase in the case of a 2-phase material with spherical particles [3]. SC+MT provides a reasonable estimation at early ages, but the estimated Young's modulus of 25.8 GPa for a mature mortar is much lower than the value experimentally measured that will be shown in the next section. Thus, SC+MT is not recommended. The DIF+DIF and DIF+GSCS schemes give almost the same estimations, and the SC+GSCS and DIF+MT schemes provide also quite close estimations. Similar conclusions can be drawn from the estimations of concrete: the schemes presented in Fig. 8(c) provide reasonable estimations including an approximation approaching 0 at early ages and values near the experiments at later ages. Therefore, they will be applied in the following simulations, keeping in mind that a confrontation with experimental data is ultimately required to select the best candidate.

4.1.2. Comparisons to experimental measurements

Firstly, we propose to compare the estimations of mechanical properties obtained with our model to experimental data on cement pastes from literature. Indeed, no such measurements have been made within our project on the investigated materials. Although the phase assemblages may have some differences, we consider it relevant and very instructive to confront the Young's modulus of cement pastes with a w/c of 0.40, 0.45, 0.50, and 0.60 estimated by using the DIF and the SC scheme, to the measured values of CEM I materials in [68] at 56 days, i.e. near to full hydration. The results of the comparison is presented in Fig. 9. It is clearly shown that the DIF scheme provides estimations close to the experimental data, while the values are significantly underestimated by the SC scheme. The underestimation of the Young's modulus via the SC scheme has been reported in the literature (see e.g. [76, 78, 79]), and is attributed to i) the fact that it is not well adapted to microstructures with matrix/inclusion morphology, ii) the existence of high property contrasts between the matrix and the inclusive phases and the significant volume fractions of the latter [79], especially at the level of cement paste. Therefore, in the following the DIF scheme is selected to simulate the mechanical properties of cement paste.

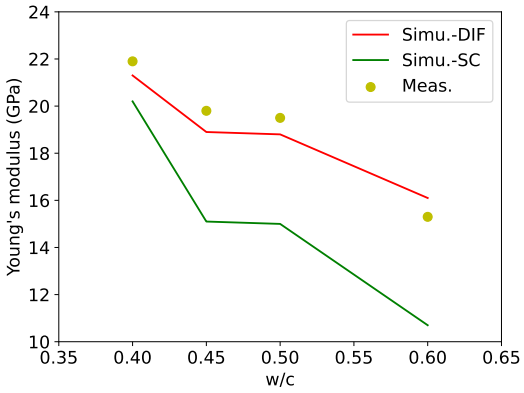

Figure 9: Comparison of the estimated Young's modulus of the cement paste with a w/c of 0.40, 0.45, 0.50, and 0.60 after 56 days of hydration to the measured values in [68].

Next, within the project the dynamic elasticity moduli of mortars prepared with the CEM II/C-M (S-LL) binder and various w/c ratios (0.40, 0.50, and 0.60) at 20 °C have been determined with a non-destructive method according to EN 843-2 [80]. The dynamic elasticity modulus of the mortar, E_d, can be calculated with the equation [81]:

$$E_d = \frac{1}{t^2} \times l^2 \times \rho \times C_L \tag{3}$$

where E_d is in N/mm^2, t is the running time of the emitted sound impulse in μs, l is the length of tested prisms ($l = 160$ mm), ρ is the density of materials in kg/m^3, and C_L is a coefficient around 0.9 [81]. Then, the calculated dynamic moduli are converted to static ones, E_s, using the following formula:

$$E_s = E_d \left(1 - ae^{-bE_d}\right) \tag{4}$$

where a and b are two parameters depending on the w/c and the curing temperatures [82]; $a = 0.4920$ and $b = 0.0177$ mm^2/N are taken from this reference, in which measurements were performed on concrete samples prepared with CEM I and a w/c of 0.50, hydrated at a temperature of 23 °C.

The static elasticity moduli converted from dynamic ones are presented in Fig. 10, together with the simulations estimated by the DIF+DIF scheme. The DIF+GSCS scheme provides quite similar estimations to the ones via the DIF+DIF scheme, with a maximum absolute deviation of 0.8%. The results estimated by the SC+SC, SC+GSCS, and DIF+MT schemes are lower than the ex-

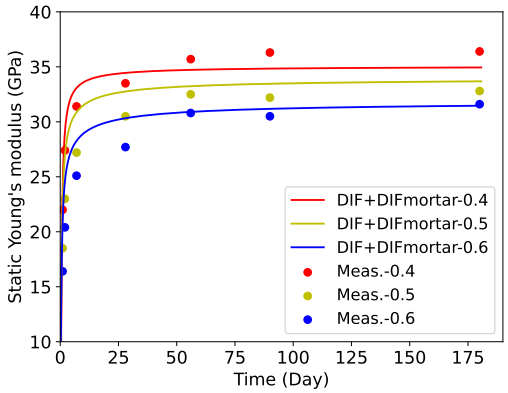

Figure 10: Comparison of the estimated and measured Young's modulus of the mortar with w/c=0.40, 0.50, and 0.60.

perimental data, and thus are not illustrated in this figure but added in Appendix C. The only difference for these three mortars comes from the GEMS simulations that provide different amounts of hydration phases in cement paste. Among the multiple analytical schemes that have been tested, the DIF+DIF and DIF+GSCS schemes turn out to provide the estimations which are the closest to the measurements, based on simple 1-level representative microstructures adopted in this study. The Young's moduli of the mortars estimated by the DIF+DIF and DIF+GSCS schemes show a good consistency with experimental measurements, especially at later ages, while at early ages they are slightly overestimated. Note that the GEMS simulations predict quite stable phase assemblages after 20-25 days of hydration (see Fig. 1), while the experimental data of Young modulus indicate an increase of about 10-15% after this period. The average absolute deviations for the mortars with w/c of 0.40, 0.50, and 0.60 are 4.92%, 10.10%, and 10.59%, respectively. These values are reduced to 3.66%, 2.91%, and 1.08% considering the estimations after 28 days, which are of more interest from the viewpoint of the long-term performance of materials.

4.2. Diffusive properties

The diffusive properties upon hydration of cement paste estimated via the MT, SC, and DIF schemes, as well as the subsequent diffusive properties for mortars and concretes estimated by the GSCS are summarized in this section. The diffusion coefficient of cement paste prepared with the

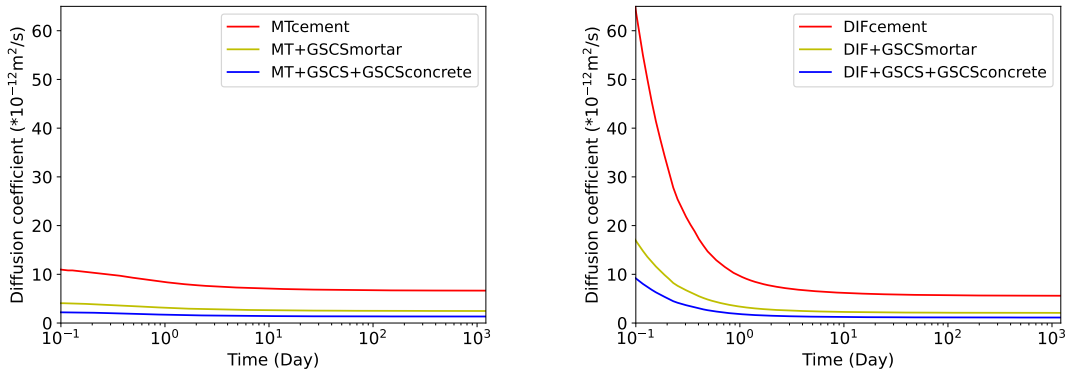

(a) Estimated diffusion coefficients of materials by the MT+GSCS+GSCS scheme;

(b) Estimated diffusion coefficients of materials by the DIF+GSCS+GSCS scheme.

Figure 11: Estimated diffusion coefficients of materials with the CEM II/C-M (S-LL)-0.50 binder at 20 °C via (a) the MT+GSCS+GSCS scheme and (b) the DIF+GSCS+GSCS scheme.

CEM II/C-M (S-LL)-0.50 binder hydrated at 20 °C estimated by the SC scheme is close to 0, which proves that the SC scheme is not suitable to estimate the diffusive properties with the 1-level representative microstructure adopted in this work. The diffusion coefficients for the materials at different scales estimated by the MT+GSCS+GSCS and DIF+GSCS+GSCS schemes are presented in Fig. 11. The main differences between these two estimations are within the first day of hydration. At later ages the diffusion coefficients of cement paste estimated using the MT and DIF schemes are similar, with values around 6.65×10^{-12} m^2/s via the MT scheme and 5.60×10^{-12} m^2/s via the DIF scheme. These estimations are close to the experimental results reported in [83], where the diffusion coefficient has been measured as 6.81×10^{-12} m^2/s for cement paste with type 10 Portland cement and a w/c of 0.50. At the scale of mortar, DIF+GSCS tends to give higher estimations at the early-age and lower values at later ages, compared to the ones estimated by the MT+GSCS scheme. After 1215 days of hydration, the estimated diffusion coefficients of mortar are 2.47×10^{-12} m^2/s by the MT scheme and 2.08×10^{-12} m^2/s by the DIF scheme, and those for concretes are estimated as 1.34×10^{-12} m^2/s by the MT scheme and 1.13×10^{-12} m^2/s by the DIF scheme. The estimations at different scales show as expected a decreasing trend from cement paste to mortar, and subsequently to concrete, which is caused by the addition of non-diffusive

aggregates. This decreasing trend of diffusion coefficients from cement paste to mortar has been reported in numerous studies, e.g. [84] among others.

4.3. 3D simulations

In this subsection, we propose to compare the analytical estimations presented above to 3D numerical simulations to help selecting (or confirm) the best estimation procedure. The main motivation is that such simulations performed on representative microstructures provide accurate results that may be used with confidence to validate the analytical methods. To date, limited numerical data are available in particular in the case of composite spheres exhibiting a layer as considered in this study, and complementary 3D results are expected to be of significant interest in this regard. Here the numerical simulations are performed with the finite element (FE) method on 3D specimens consisting of a homogeneous matrix, in which spherical particles surrounded by a layer of given thickness are embedded. These specimens are designed to mimic mortar, i.e. composite spheres of sand grains surrounded by an ITZ and distributed in the homogeneous cement paste. Three realizations of periodic microstructures are used with the same number and sizes of particles and layer thickness, the only difference being their random placement in the box. The procedure leading to the generation of the microstructure geometries by the CAD platform Salome [85], and the subsequent mesh created by automatic meshing softwares developed by Distene [86] is described in details in e.g. [35, 87] and references therein. For more information, the interested reader is invited to refer to these publications. With the assumptions that the ITZ thickness is 16 μm and the volume fraction of hydrates and capillary pores in cement paste transferred to the ITZ is 7.3%, the mortar fabricated with the CEM II/C-M (S-LL)-0.5 binder has a composition of 53.7 vol.% of sand, 3.5 vol.% of ITZ, and 42.8 vol.% of cement paste at early ages. To limit the mesh size, the microstructures are generated with a lower volume fraction of composite inclusions than in the mortar sample mentioned above: 37.82% and 3.31% for the particles and ITZ, respectively. In addition, we have assigned the value of 0.04 mm to the ITZ rather than 0.016 mm that we have employed in the above simulations. This is deemed to be inconsequential with regard to our comparison objective, since the input in the estimation procedure can be very easily changed. The number of spherical particles is set to 545, with diameter size ranging from 0.1 to 2 mm, to be related to the box size whose edge dimension is 10 mm, and the ITZ thickness is fixed to 0.04 mm for all particles. Fig.

12 shows the mesh of such a generated microstructure, exhibiting 5.41×10^6 tetrahedral elements. The 2 other meshes have comparable sizes with 5.42×10^6 and 5.46×10^6 elements. The simulations are performed with the FE code Cast3M developed at CEA [88]. Periodic boundary conditions (BC) are applied on the sample surfaces, as they are generally known to lead to results closer to the real properties than uniform BC. In this regard, simulations were also conducted with both uniform stresses and strains BC, and the results (not shown) in terms of overall elastic properties exhibited a maximum difference of 2%, meaning that the representativeness of the generated microstructures is satisfactory. The computation times are of the order of 45 min and 20 min for solving the mechanical and diffusion problems with Periodic BC (about 20 min and less than 10 min for homogeneous BC), respectively.

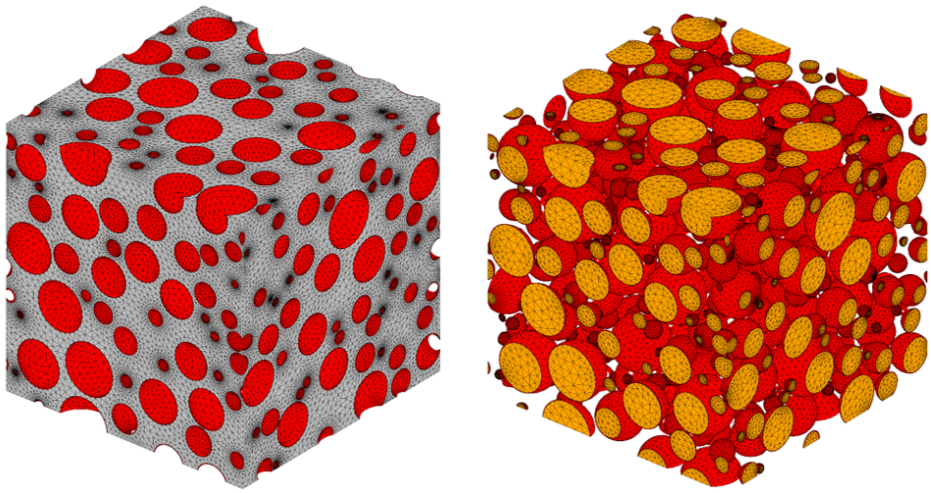

(a) (b)

Figure 12: Example of a realization of a microstructure generated with 37.82% and 3.31% of volume fraction of particles and ITZ layer, respectively, whose mesh exhibits a total of 5.41 millions of tetrahedral elements.

The values of the mechanical and diffusive properties that have been used in the simulations are summarized in Table 5. To increase the confidence of the comparison, 4 configurations have been tested with different properties for both cement paste and ITZ, corresponding to various times of hydration ranging from 1 to 1215 days, the latter date being very close to the final hydration state. The compositions are based on the phase assemblage of the CEM II/C-M (S-LL)-0.5 binder that has been illustrated in Fig. 1(b). The values of the properties are estimated by the analytical pro-

Table 5: Values of elastic and diffusive properties used in the simulations.

Hydration time	Materials	Young's modulus (GPa)	Shear modulus (GPa)	Diffusive property ($\times 10^{-12}$ m^2/s)
1 day	Cement paste	13.6	5.3	8.35
	ITZ	2.7	1.3	14.40
	Sand	70	26.9	0
2 days	Cement paste	15.6	6.2	7.75
	ITZ	3.9	1.8	13.10
4 days	Cement paste	16.9	6.7	7.38
	ITZ	4.9	2.2	12.30
1215 days	Cement paste	19.1	7.6	6.65
	ITZ	7.9	3.4	10.60

cedure described in section 3; note that as the properties of sand are constant with time, they are only reported once in Table 5. To be more specific, the mechanical properties of cement paste and the ITZ are estimated by the DIF and the SC scheme, and their diffusive properties are estimated by the MT scheme. The simulation results are compared to the analytical estimations obtained with DIF+GSCS and DIF+ DIF methods, except for diffusive properties where only MT+GSCS is applied. Fig. 13 shows the comparison in terms of Young's modulus (a) and diffusion coefficient (b). The numerical points are obtained by averaging the simulated data for the 3 generated specimens. However, it is worth mentioning that the maximum differences between the 3 numerical values are less than 0.1 and 0.25% for mechanical and diffusive properties, respectively, confirming that the representativeness of the 3D numerical procedure is good. We observe that the analytical estimations are in close agreement with the numerical results, especially for the Young's modulus where the discrepancies are generally less than 1% (except for one point with DIF+GSCS), while they range between 1.1 and 1.7% for the diffusion coefficient. The DIF+DIF estimations of mechanical properties are slightly closer to the simulation results than DIF+GSCS ones, with a maximum difference of 0.5%. To conclude, the 3D simulations performed in this subsection have allowed the collection of valuable data that could serve as a benchmark for estimation procedures. Clearly, the analytical methods proposed in the previous sections to deal with microstructures exhibiting aggregates surrounded by an ITZ appear very convincing as the corresponding analytical estimates of both elastic and diffusive properties are very close to the simulations results. The adequacy of the estimation procedures reported in section 4.1.2 through the comparison with experimental data is also confirmed by the confrontation with the 3D simulation results.

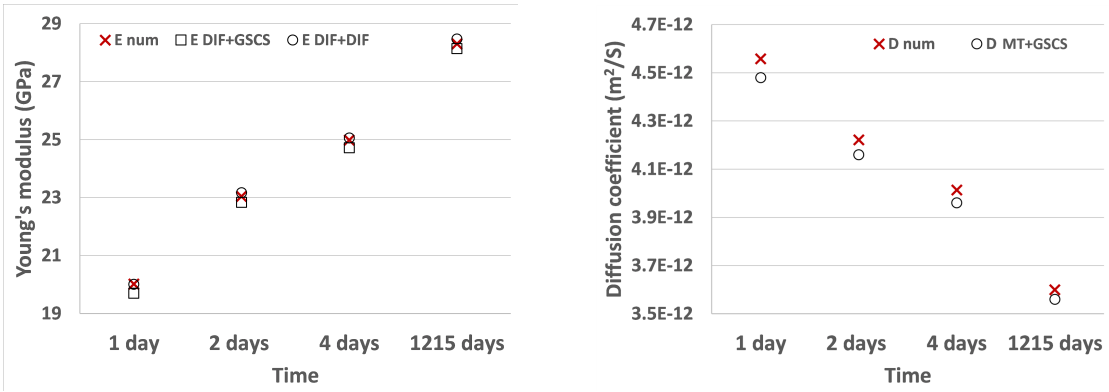

(a) (b)

Figure 13: Comparison between simulation results (red crosses) and analytical estimations (squares and circles) for (a) Young modulus and (b) diffusion coefficient.

4.4. Analyses of the ITZ effects

In this subsection we propose to analyze the effects of the assumptions made for describing the ITZ on the estimated results. As explained in section 3.2.2, we retained the following parameters for the ITZ: its thickness is set to 16 μm; a volume fraction (α) of hydrates and capillary pores in cement paste is transferred to the ITZ and the remaining space of the ITZ is occupied by pores. Without supplementary information regarding the materials, we tested several values and $\alpha = 7.3\%$ turns out to give satisfactory estimations. With these assumptions, the mortar fabricated with the CEM II/C-M (S-LL)-0.50 binder has a composition of 53.7% of sand, 42.8% of cement paste, and 3.5% of ITZ in volume after 1215 days of hydration. We will use the SC and the MT scheme to estimate the mechanical and diffusive properties of the ITZ, respectively, since it has been proved previously that these two schemes provide reliable estimations for the cement paste, which is the main component of the ITZ. The porosity of the ITZ is around 50.9% at later ages, and its estimated Young's modulus and shear modulus are 10.03 and 4.18 GPa via the SC scheme, i.e. approximately half of the ones of the matrix phase as in e.g. [23, 89]. Under the same state, the estimated diffusion coefficient of the ITZ via the MT scheme is around 9.87×10^{-12} m^2/s, which is 3.99 times higher than the one of the mortar. Ratios of the diffusion coefficient of the ITZ to the one of the mortar have been reported as 2.83 in [90], 3.62 and 5.84 in [91], which are close to

the value in this study. Moreover, the comparison of the estimated Young's modulus of mortar with the experimental measurements proved to be consistent, see section 4.1.2. These reasonable estimations then validate the assumption to transfer 7.3 vol% of hydrates and capillary pores in cement paste to the ITZ that has a thickness of 16 μm.

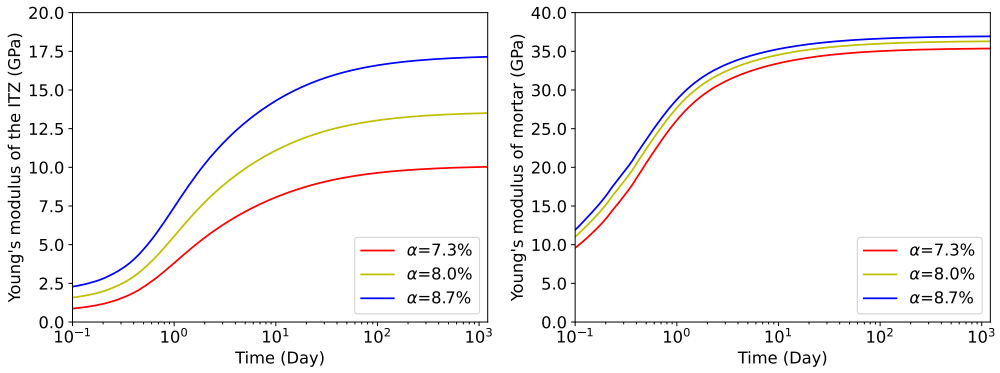

(a) Estimated Young's moduli of the ITZ; (b) Estimated Young's moduli of the mortar.

Figure 14: Estimated Young's moduli of (a) the ITZ via the SC scheme and (b) the mortar via the DIF+DIF scheme with various volume fractions (α) of hydrates and capillary pores transferred from the cement paste to the ITZ in mortar: $\alpha = 7.3\%$, 8.0%, and 8.7%.

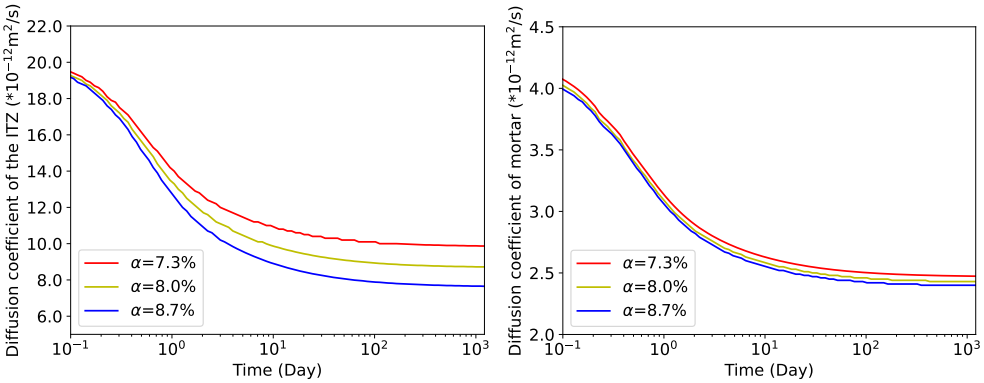

(a) Estimated diffusion coefficients of the ITZ; (b) Estimated diffusion coefficients of the mortar.

Figure 15: Estimated diffusion coefficients of (a) the ITZ via the MT scheme and (b) the mortar via the MT+GSCS scheme with various volume fractions (α) of hydrates and capillary pores transferred from the cement paste to the ITZ in mortar: $\alpha = 7.3\%$, 8.0%, and 8.7%.

To better understand the effect of the ITZ composition on its properties, two additional volume

fractions (α) of the hydrates and capillary pores transferred from the cement paste to the ITZ are considered: 8.0% and 8.7%. These variations have little effect on the porosity of the mortar, e.g. it decreases from 0.292 to 0.286 with the increasing α at later ages, and therefore we will consider that the mortar has a constant porosity. Figs. 14 and 15 show the estimated Young's moduli and diffusion coefficients of the ITZ and the mortar with various α. It is observed that a higher volume fraction of the hydrates and capillary pores transferred from the cement paste to the ITZ contributes to a higher estimated Young's modulus and a lower diffusion coefficient of the ITZ, especially at later ages. However, its effect on the mechanical and diffusive properties of the mortar is relatively weak. This can be explained by the fact that with a fixed ITZ thickness of 16 μm, a higher volume fraction of the hydrates and capillary pores transferred to the ITZ leads to a less porous microstructure of the ITZ. As expected, the mechanical and diffusive properties of the ITZ and the mortar highly depend on the assumptions made for their respective composition and arrangement, and also on the schemes used. However, without sufficient experimental data for the ITZ in this study, the assumption of 7.3 vol% of the hydrates and capillary pores in cement paste transferred to the ITZ gives quite reasonable and relevant estimations concerning the Young's moduli and the diffusive coefficients of the ITZ and the mortar, hence it is adopted here.

The effect of the ITZ thickness (h) on the Young's modulus and diffusion coefficient of the ITZ and the mortar is now investigated, and three values of thickness (h) are considered: 16, 20, and 24 μm. Correspondingly, the porosity of mortar increases slightly from 0.292 to 0.305. Figs. 16 and 17 present the comparison of the estimated Young's moduli and diffusion coefficients of the ITZ and the mortar with various h. It can be concluded that h has non-negligible effects on the mortar's property at early ages and a significant effect at later ages. Due to the simple hypothesis of a fixed radius of the fine aggregate (0.75 mm), increasing h from 16 to 24 μm leads to increasing the volume fraction of the ITZ in mortar from 3.5% to 5.2%. Consequently, reduced volume fractions of the bulk paste in mortar are obtained, which have higher Young's moduli and lower diffusion coefficients than those of the ITZ. Furthermore, a greater h leads to a more porous structure of the ITZ, giving in turn a lower Young's modulus (see Fig. 16(a)) and a higher diffusion coefficient (see Fig. 17(a)). The fact that varying h has more impact on the Young's modulus of the ITZ and the mortar than on their diffusion coefficients is mainly attributed to the use of different upscaling schemes: SC scheme and MT scheme for mechanical and diffusive properties, respectively. To summarize, an

increased volume fraction associated with a more porous structure of the ITZ in mortar are the reasons for the fact that $h = 24$ μm leads to the lowest Young's modulus and the highest diffusion coefficient of the mortar compared to the other values of h.

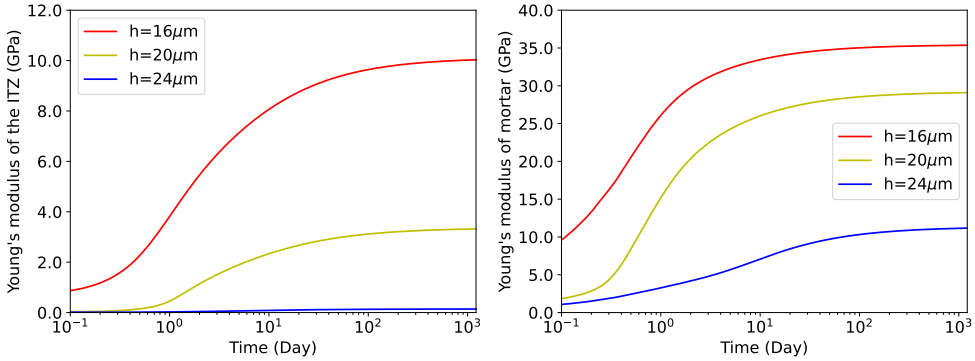

(a) Estimated Young's moduli of the ITZ; (b) Estimated Young's moduli of the mortar.

Figure 16: Estimated Young's moduli of (a) the ITZ via the SC scheme and (b) the mortar via the DIF+DIF scheme with various ITZ thicknesses: h =16, 20, and 24 μm.

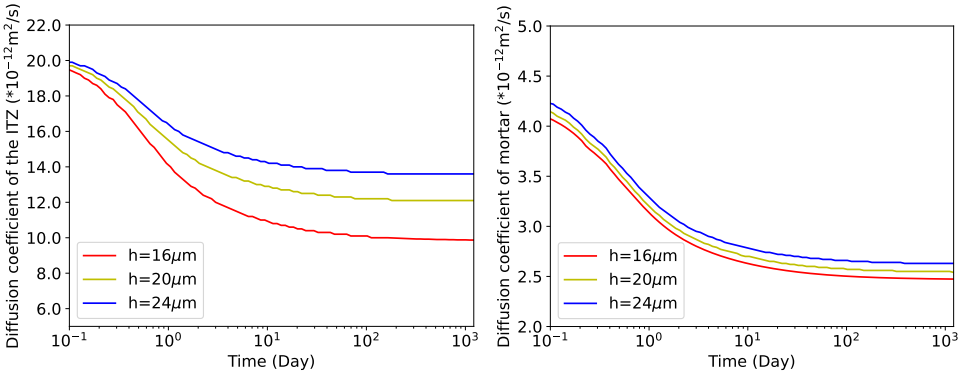

(a) Estimated diffusion coefficients of the ITZ; (b) Estimated diffusion coefficients of the mortar.

Figure 17: Estimated diffusion coefficients of (a) the ITZ via the MT scheme and (b) the mortar via the MT+GSCS scheme with various ITZ thicknesses: h =16, 20, and 24 μm.

To conclude, among the different parameters characterizing the ITZ in this study, h appears to be the most influential one, especially on the mechanical properties of materials. The assumptions retained for these parameters are deemed to provide reasonable estimations of the material properties.

5. Estimations of the degraded materials properties

In this section, the estimations of the mechanical and diffusive properties of materials exposed to carbonation, leaching with water and solutions containing chloride ions are presented. The DIF+DIF/GSCS schemes, which are recommended as the schemes providing the estimations of mechanical properties the closest to the experimental measurements and 3D analyses, are applied. Since DIF+DIF(+DIF) and DIF+GSCS(+GSCS) schemes provide quite close estimations, only the data from the DIF+DIF(+DIF) scheme will be shown in the figures. The diffusion coefficients of materials are estimated by the MT+GSCS(+GSCS) scheme.

5.1. Materials exposed to carbonation

We estimate in this section the properties of materials exposed to a progressive carbonation as described in section 3.1 after 76 days of hydration. The total volume fraction of capillary water and the space due to chemical shrinkage in the hydrated binders at 76-day is assumed to be the initial capillary porosity. With the addition of CO_2, hydration phases decompose, and the porosity is assumed to be always saturated with water. Fig. 18 shows the evolution of the total porosity and the capillary porosity in CEM II/C-M (S-LL)-0.60 as a function of the formed calcite during carbonation. The total porosity remains almost constant with a slight decrease and subsequent increase between about 15 and 30 cm^3 of formed calcite per 100 g of binder. Different variations of the total porosity after carbonation have been reported in the literature: a reduction of the total porosity has been found for Portland cement paste [92, 93, 94] and an increase of total porosity has been observed for Portland cement with supplementary cementitious material blends [92, 95, 96]. Moreover, the microstructure of cement paste has been found rearranged after carbonation [97] with a shift towards larger pores and an increased ratio of capillary porosity with respect to total porosity [94], which is consistent with the results presented in Fig. 18. The occurrence of microcracks may be another reason to the increased size of pores [98]. Note that the GEMS results cannot predict microcracks appearance nor provide direct data on the pore size evolution during chemical reactions, since the prediction of the spatial distribution of phases and their volumes are not available in thermodynamic modeling.

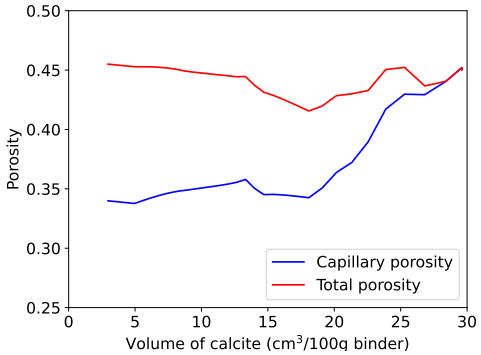

Figure 18: Evolution of the total porosity and capillary porosity of the cement paste with CEM II/C-M (S-LL)-0.60 at 20 °C as a function of the volume of formed calcite in $cm^3/100$ g of binder.

Comparisons between the total porosity of materials after carbonation predicted by thermodynamic modeling and obtained experimentally have been made in several studies in the literature. A higher total porosity in carbonated materials predicted by thermodynamic calculations compared to the value measured by MIP has been reported in [40, 41]. It can be explained by the fact that mercury is not accessible to closed pores in materials on the one hand, and on the other hand that thermodynamic calculations are based on the material after completed carbonation. [43] have compared the total porosity measured by MIP with the one calculated by thermodynamic model taking into account the actual carbonation degree that was experimentally measured by TGA, and found out that the results are quite close. The discrepancy has been found to be further reduced when considering the additional hydration of clinker. The authors have explained that the minor discrepancy comes from the facts that: (i) in general, thermodynamic modeling is performed at equilibrium and then assumes that carbonation starts from the least stable phase, and processes to next reaction when the previous one is completely finished, which is different from the reality where all reactions occur simultaneously; (ii) thermodynamic model assumes that reactant hydrates carbonate completely, while in reality a part of certain hydrates may keep uncarbonated; (iii) different densities and chemical compositions in some phases may have been considered. To sum up, we can consider that the porosity calculated by the thermodynamic model is trustworthy.

Fig. 19 presents the estimated mechanical and diffusive properties of the materials with CEM II/C-M (S-LL)-0.60 binder at 20 °C as a function of (1) the added quantity of CO_2 (down axis), and (2)

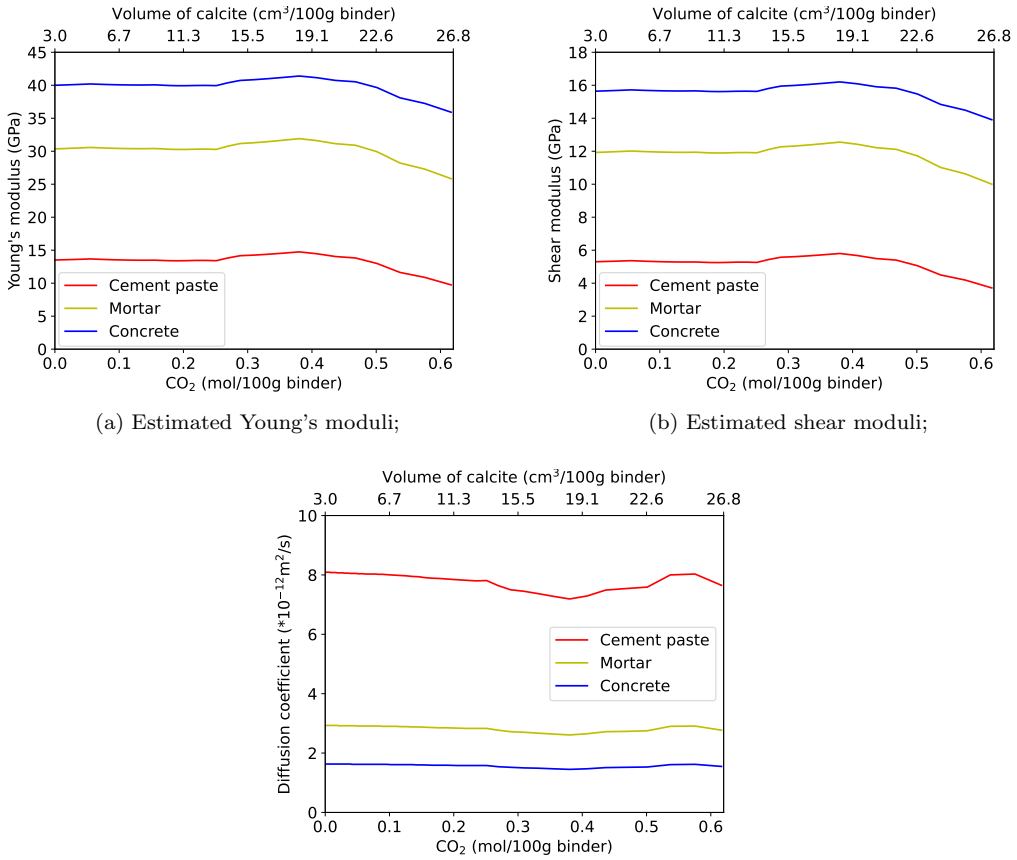

(a) Estimated Young's moduli;

(b) Estimated shear moduli;

(c) Estimated diffusion coefficients.

Figure 19: Estimated mechanical properties via the DIF+DIF+DIF scheme and diffusive properties via the MT+GSCS+GSCS scheme of the materials with the CEM II/C-M (S-LL)-0.60 binder exposed to CO_2.

the corresponding volume of formed calcite (top axis), up to approximately 0.62 mol, after which C-S-H is totally depleted and the homogenisation procedure is no more applicable. These materials show almost constant moduli up to about 0.25 mol CO_2 added (i.e. 13.3 cm^3/100 g binder of calcite is formed), due to the replacement of portlandite firstly and subsequently of C-S-H by calcite, with a concomitant release of water. Then, the moduli increase slightly because of the formation of zeolites and ferrihydrite when CO_2 is added up to about 0.38 mol (calcite is formed up to 18 cm^3/100 g binder), with the decalcification of C-S-H going on. The continuous transformation of C-S-H into calcite, which releases water, contributes to the decrease of the modulus until all C-S-H is consumed. Moreover, due to the concomitant decrease of C-S-H and increase of pores

(two diffusive phases), the materials exposed to carbonation exhibit an almost constant diffusion coefficient of 7.96×10^{-12} m^2/s for cement paste, 2.89×10^{-12} m^2/s for mortar, and 1.61×10^{-12} m^2/s for concrete. Interestingly, a competing effect between porosity clogging, which leads to a decrease in transport property, and microcracking due to carbonation shrinkage, has been reported in e.g. [99, 100, 101]. Moreover, the porosity of cement paste in this study is stable around 0.45 before and after exposure to CO_2, and the chloride diffusion coefficient of cement pastes having a similar porosity has been simulated to 7.13×10^{-12} m^2/s for a porosity of 0.44 and 7.57×10^{-12} m^2/s for a porosity of 0.46 in [11], which are close to the estimation in Fig. 19(c).

5.2. Materials exposed to leaching with water and chloride containing solutions

We investigate in this subsection the effects of leaching with pure H_2O and exposure to a solution containing chlorides on the evolution of both mechanical and diffusive properties, based on the phase assemblage calculated by thermodynamic modeling. As in the previous section, we assume that the initial state of materials is determined from the hydration simulation with GEMS, at 146 days. With the addition of solution, hydrated phases decompose (and possibly transform to other phases), which increases the porosity.

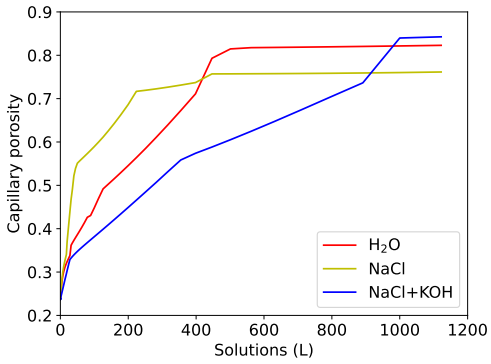

Figure 20: Comparison of the capillary porosity of the CEM II/C-M (S-LL)-0.45 binder exposed to leaching with water, NaCl, and NaCl+KOH solutions.

Fig. 20 presents the evolution of the capillary porosity of the CEM II/C-M (S-LL)-0.45 binder exposed to leaching with water and NaCl (+KOH) solutions. Of all three exposures, the porosity

increases the fastest in the case of NaCl. This means *a priori* that this solution causes the fastest degradation rate of mechanical properties, and the fastest increase of diffusion coefficient. When the cement paste is exposed to leaching with water, less degradation due to leaching predicted by the thermodynamic model at a given added volume compared to the exposure to NaCl, where C-S-H is predicted to decompose faster to form zeolites. Besides, materials exposed to NaCl+KOH shows the lowest degree of leaching. As expected, the presence of KOH considerably reduces the leaching effects and the associated porosity changes for volumes below 1000 L, which contributes to a lower degradation rate of the material. However, the exposure to NaCl+KOH leads to a higher porosity of around 0.84 for volumes higher than 1000 L, compared to the exposure to NaCl solution where porosity reaches around 0.76 due to the formation of M-S-H and zeolite in the late stage of exposure.

Fig. 21 presents the estimated Young's modulus, shear modulus, and diffusion coefficient of the materials with CEM II/C-M (S-LL)-0.45 plotted as a function of the added volume of H_2O (lower axis), and of the corresponding volume of CH+C-S-H solid (top axis). CH and C-S-H are indeed often considered as an indicator of the degradation level when exposed to leaching. The Young's moduli of the materials with the CEM II/C-M (S-LL)-0.45 binder start from the values of 42.9 GPa for concrete, 33.7 GPa for mortar and 17.9 GPa for cement paste, and decrease to nearly 0 when 500 L of H_2O is added, at which point all portlandite and C-S-H have dissolved. Besides, the dissolution of hydrates contributes to an increase of diffusion coefficient from 5.95×10^{-12} m^2/s to 1.67×10^{-11} m^2/s for cement paste, 2.15×10^{-12} m^2/s to 5.90×10^{-12} m^2/s for mortar, and 1.18×10^{-12} m^2/s to 3.22×10^{-12} m^2/s for concrete. Thus, the diffusion coefficient of cement paste after leaching is increased by a factor of approximately 2.8. Interestingly, an increase by a factor of 2.90 of the diffusion coefficient of cement paste (with w/c=0.60) due to leaching has been reported in [102]. Note that comparing our estimations with measurements in literature is challenging since little information about the degradation degree is generally available; in particular, the data may be obtained on materials that are non homogeneously degraded.

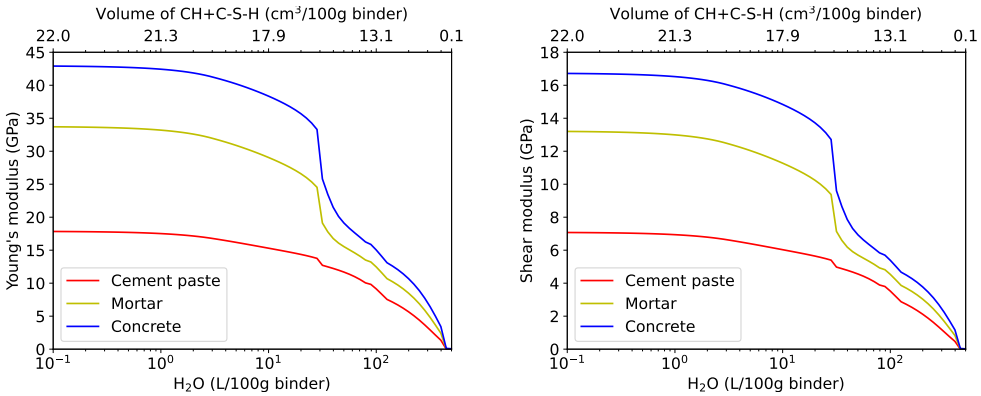

(a) Estimated Young's modulus;

(b) Estimated shear modulus;

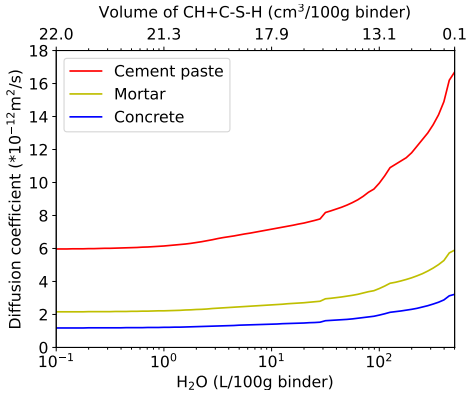

(c) Estimated diffusion coefficient.

Figure 21: Estimated mechanical properties via the DIF+DIF+DIF scheme and diffusive properties via the MT+GSCS+GSCS scheme of the materials with the CEM II/C-M (S-LL)-0.45 binder exposed to leaching, as a function of the volume of H_2O added (down axis) and the corresponding volume of CH+C-S-H solid (top axis).

Fig. 22 presents the estimations of the mechanical and diffusive properties of the materials with the CEM II/C-M (S-LL)-0.45 binder exposed to a 3% NaCl solution up to 200 L in the left column and to a 3% NaCl+KOH solution up to 1122 L in the right column at 20 °C, as a function of the added volume of solution (down axis) and of the volume of CH and C-S-H solids on the top axis. The addition of a large amount of NaCl solution affects the hydrated phases, and the associated leaching phenomenon weakens the mechanical properties of the materials. Before exposure, the initial Young's moduli and diffusion coefficients of concrete, mortar, and cement paste are the same as in Fig. 21. The Young's moduli decrease slightly for added volumes of NaCl solution up to 18

L (16 cm^3/100 g CH+C-S-H is left), and continue to decrease considerably afterwards. Moreover, the materials have a higher diffusion coefficient with the addition of NaCl solution: the estimated maximum diffusion coefficients for cement paste, mortar, and concrete are 1.56×10^{-11} m^2/s, 5.24×10^{-12} m^2/s, and 2.82×10^{-12} m^2/s, respectively. For comparison, the diffusion coefficient of a CEM I cement paste with w/c=0.53 and an initial porosity of 0.48 exposed to a 3% NaCl solution has been measured by steady-state accelerated chloride diffusion test method in [11], and the value of 1.06×10^{-11} m^2/s has been reported. After 25 L of added NaCl solution, the porosity of the cement paste in our study is around 0.50, and the estimated diffusion coefficient is around 9.55×10^{-12} m^2/s, which is quite close to the cited measured value.

With the presence of KOH, the leaching attack on the hydrated cement is significantly slowed down compared to the case of NaCl solution; for instance, materials have degraded largely when 18 L of NaCl solution (or more) are added, while to obtain an equivalent level of degradation with the addition of KOH+NaCl, more than 100 L of solution is required. During the exposure to 3% NaCl+KOH, the diffusion coefficients increase up to 1.73×10^{-11} m^2/s for cement paste, 6.13×10^{-12} m^2/s for mortar, and 3.35×10^{-12} m^2/s for concrete.

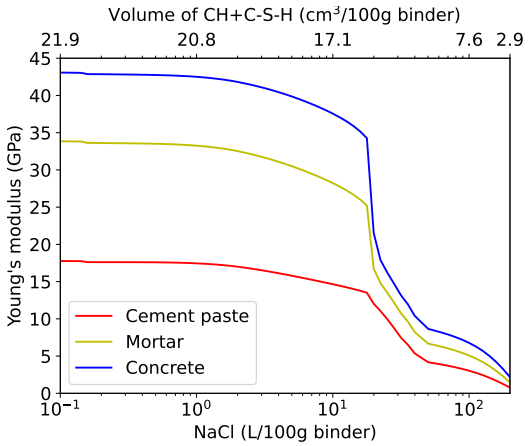

(a) Estimated Young's moduli - 3% NaCl;

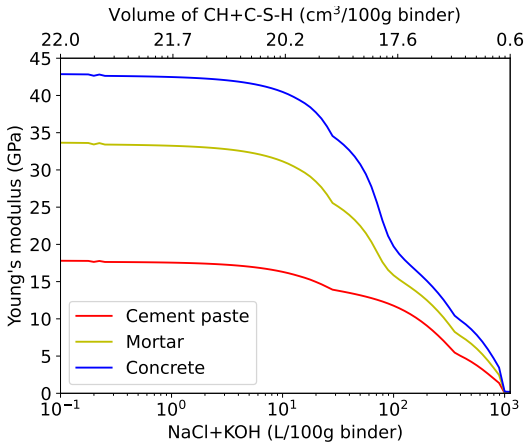

(b) Estimated Young's moduli - 3% NaCl+KOH;

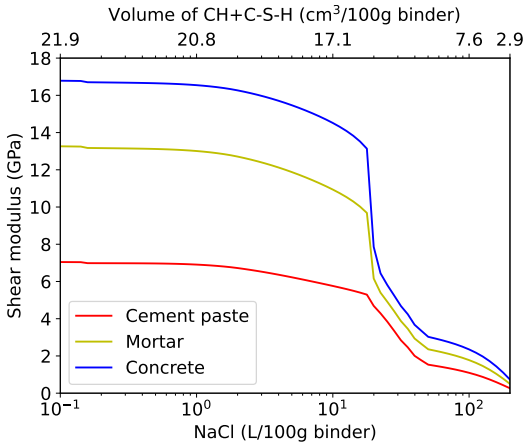

(c) Estimated shear moduli - 3% NaCl;

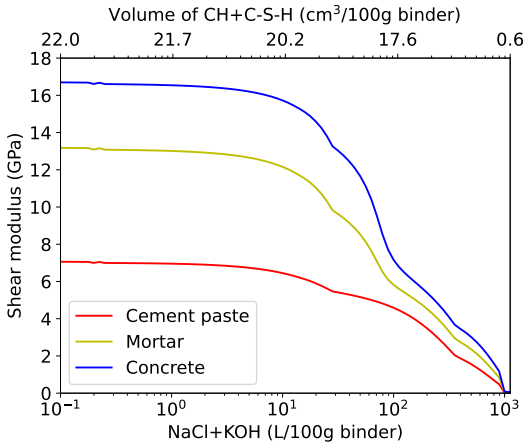

(d) Estimated shear moduli - 3% NaCl+KOH;

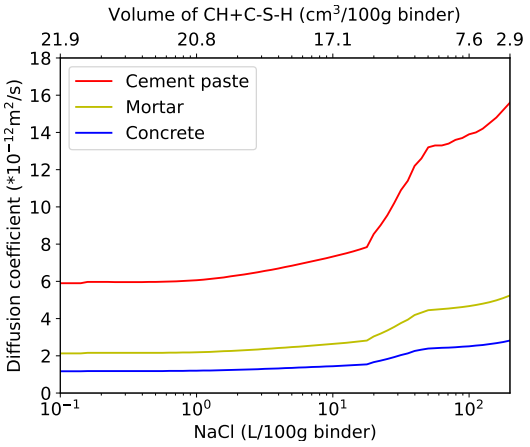

(e) Estimated diffusion coefficients - 3% NaCl;

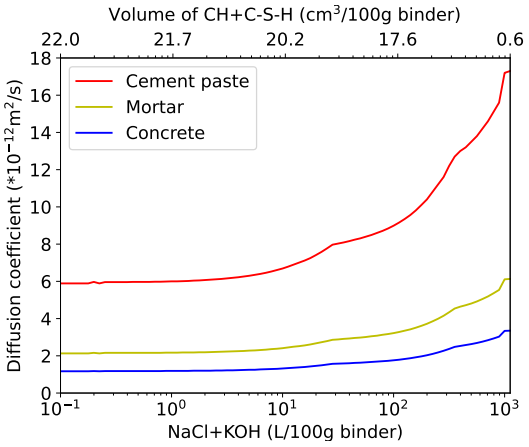

(f) Estimated diffusion coefficients - 3% NaCl+KOH.

Figure 22: Estimated mechanical properties via the DIF+DIF+DIF scheme and diffusive properties via the MT+GSCS+GSCS scheme of the materials with the CEM II/C-M (S-LL)-0.45 binder exposed to 3% NaCl (left) and to 3% NaCl+KOH (right) solutions at 20 °C.

6. Conclusions

In this work, a procedure for estimating the mechanical and diffusive properties of materials made with a novel CEM II/C-M (S-LL) binder has been presented. The phase assemblage of the binder upon hydration and when further exposed to carbonation, leaching with water and chloride containing solutions (3% NaCl and 3% NaCl+KOH), has been calculated using thermodynamic modeling. Then, both mechanical and diffusive properties of the materials have been studied at different scales: cement paste, mortar, and concrete. Three classical analytical approximation schemes, namely the Mori-Tanaka, the self-consistent, and the differential schemes, have been applied to estimate the properties of cement paste, based on a simplified one-level representative microstructure where hydrates, anhydrous phases, capillary water, and empty pores are considered as spherical inclusions randomly distributed. A replacement procedure combined with one of the above classical schemes, and the generalized self-consistent scheme have been adopted to estimate the properties of mortar and concrete.

The ITZ in mortar and concrete is assumed to be composed of a volume fraction of hydrates and capillary pores transferred from the cement paste. Three different values (7.3%, 8.0%, and 8.7%) have been considered, the higher one contributing to a higher estimated Young's modulus and a lower diffusion coefficient of the ITZ, especially at later ages. The effects of the ITZ thickness on the mechanical and diffusive properties of the ITZ and mortar have also been studied. An increasing thickness leads to a decrease of Young's moduli of the ITZ and the mortar, and an increase in their diffusion coefficients with a lesser impact. For mortar and concrete, an ITZ thickness of 16 μm and 7.3 vol% of hydrates and capillary pores transferred from the cement paste is assumed. Based on these assumptions, the DIF+DIF and DIF+GSCS schemes, which give very similar estimations, turn out to provide the estimation that best match the experimental Young's modulus of mortar. Moreover, a 3D computational analysis performed on microstructures composed of spheres surrounded by a thin layer representing the ITZ has allowed for the calculation of the mechanical and diffusive properties of mortar-like materials. The numerical results obtained have shown good consistency with the analytical estimations using the DIF+DIF and DIF+GSCS schemes.

The procedure has been applied to the estimation of mechanical and diffusive properties of the

saturated materials made with the CEM II/C-M (S-LL) binder with w/c=0.60 exposed to CO_2 at 20 °C. With the addition of CO_2, the materials show first an almost constant Young's modulus followed by a decrease, due to the concomitant decalcification of C-S-H and the increased volume of capillary pores, while diffusion coefficients are moderately affected throughout the process. Next, the mechanical and diffusive properties of materials made with the CEM II/C-M (S-LL)-0.45 binder exposed to leaching with water and solutions containing either 3% NaCl and 3% NaCl+KOH have been investigated. With the exposure to increasing volumes of solutions, the hydrated phases decompose, leading to a decreasing volume of solid phases and an increasing volume of pores, and consequently contributing to a decrease in elastic modulus and an increase in diffusion coefficient. However, as expected the presence of KOH postpones the leaching process, and an equivalent mechanical degradation is obtained for a higher volume of exposure solution compared to the case with only NaCl. The NaCl solution leads to the fastest degradation of mechanical properties and the fastest increase of diffusion coefficient, while the porosity reached after being exposed to leaching with water and NaCl+KOH solution is slightly higher.

In the future, a deeper comparison of the estimated properties in the considered degradation cases would help increase the confidence and validate the proposed methodology. However, such task appears extremely difficult since it would require homogeneous states of degradation at various levels within specimens, which is very challenging in particular for concrete. Moreover, an extension of the proposed approach to the estimation of physical parameters of cementitious materials in unsaturated conditions would be helpful in particular in the case of carbonation, since CO_2 preferentially migrates through the gaseous phase. Finally, an analytical estimation procedure similar to the one presented may be applied to obtain creep mechanical properties and their various evolution as a function of hydration (ageing) and chemical degradation. Another aspect that would deserve to be investigated is to estimate the effects of microcracking on the different parameters. In particular, it would be meaningful to account for microcracking due to carbonation-induced shrinkage, since it is known to affect the material properties and in particular the transport ones. However, to be accurate it would also require to consider spatial gradients of shrinkage, since they lead to the development of tensile stresses. Such non-local effects are beyond the scope of our approaches.

7. Acknowledgements

This project has received funding from the European Union under the research and innovation program Horizon 2020, grant agreement No 760639. This publication reflects only the authors' view and the Commission is not responsible for any use that may be made of the information it contains. We would like to express our gratitude to Barbara Lothenbach (Empa/NTNU) for the fruitful discussion concerning thermodynamic modeling. We are also indebted to Aljoša Šajna (ZAG) and Lucija Hanžič (ZAG) for the discussions to which they participated and for their continuous support of this project.

References

[1] G. Bolte, M. Zajac, J. Skocek, M. B. Haha, Development of composite cements characterized by low environmental footprint, Journal of Cleaner Production 226 (2019) 503–514, https://doi.org/10.1016/j.jclepro.2019.04.050.

[2] J. W. Ju, K. Yanase, Micromechanics and effective elastic moduli of particle-reinforced composites with near-field particle interactions, Acta Mechanica 215 (1) (2010) 135–153, https://doi.org/10.1007/s00707-010-0337-2.

[3] S. Torquato, H. W. Haslach Jr, Random heterogeneous materials: microstructure and macroscopic properties, Applied Mechanics Reviews 55 (4) (2002) B62–B63, https://doi.org/10.1115/1.1483342.

[4] G. Constantinides, F. J. Ulm, The effect of two types of CSH on the elasticity of cement-based materials: Results from nanoindentation and micromechanical modeling, Cement and Concrete Research 34 (1) (2004) 67–80, https://doi.org/10.1016/S0008-8846(03)00230-8.

[5] J. C. Nadeau, A multiscale model for effective moduli of concrete incorporating ITZ water–cement ratio gradients, aggregate size distributions, and entrapped voids, Cement and Concrete Research 33 (1) (2003) 103–113, https://doi.org/10.1016/S0008-8846(02)00931-6.

[6] L. Dormieux, E. Lemarchand, D. Kondo, E. Fairbairn, Elements of poro-micromechanics applied to concrete, Materials and Structures 37 (1) (2004) 31–42, https://doi.org/10.1007/BF02481625.

[7] S. Scheiner, C. Hellmich, Continuum microviscoelasticity model for aging basic creep of early-age concrete, Journal of engineering mechanics 135 (4) (2009) 307–323, https://doi.org/10.1061/(ASCE)0733-9399(2009)135:4(307).

[8] J. Sanahuja, Effective behaviour of ageing linear viscoelastic composites: Homogenization approach, International Journal of Solids and Structures 50 (19) (2013) 2846–2856, https://doi.org/10.1016/j.ijsolstr.2013.04.023.

[9] M. Königsberger, M. Hlobil, B. Delsaute, S. Staquet, C. Hellmich, B. Pichler, Hydrate failure in ITZ governs concrete strength: A micro-to-macro validated engineering mechanics model, Cement and Concrete Research 103 (2018) 77–94, https://doi.org/10.1016/j.cemconres.2017.10.002.

[10] M. Königsberger, B. Pichler, C. Hellmich, Micromechanics of ITZ–aggregate interaction in concrete part i: stress concentration, Journal of the American Ceramic Society 97 (2) (2014) 535–542, https://doi.org/10.1111/jace.12591.

[11] G. Sun, Y. Zhang, W. Sun, Z. Liu, C. Wang, Multi-scale prediction of the effective chloride diffusion coefficient of concrete, Construction and Building Materials 25 (10) (2011) 3820–3831, https://doi.org/10.1016/j.conbuildmat.2011.03.041.

[12] E. Stora, B. Bary, Q.-C. He, On estimating the effective diffusive properties of hardened cement pastes, Transport in Porous Media 73 (3) (2008) 279–295, https://doi.org/10.1007/s11242-007-9170-z.

[13] M. Achour, F. Bignonnet, J.-F. Barthélémy, E. Rozière, O. Amiri, Multi-scale modeling of the chloride diffusivity and the elasticity of portland cement paste, Construction and Building Materials 234 (2020) 117124, https://doi.org/10.1016/j.conbuildmat.2019.117124.

[14] T. Honorio, B. Bary, F. Benboudjema, Estimation of elastic properties of cement based materials at early age based on a combined numerical and analytical multiscale micromechanics approach, in: RILEM Int. Symp. Concr. Model., Beijing, China, 2014.

[15] D. A. Kulik, Gem-selektor v3.3, available at: http://gems.web.psi.ch/.

[16] B. Lothenbach, F. Winnefeld, Thermodynamic modelling of the hydration of Portland cement, Cement and Concrete Research 36 (2) (2006) 209–226, https://doi.org/10.1016/j.cemconres.2005.03.001.

[17] T. Wagner, D. A. Kulik, F. F. Hingerl, S. V. Dmytrieva, GEM-Selektor geochemical modeling package: TsolMod library and data interface for multicomponent phase models, The Canadian Mineralogist 50 (5) (2012) 1173–1195, https://doi.org/10.3749/canmin.50.5.1173.

[18] D. A. Kulik, T. Wagner, S. V. Dmytrieva, G. Kosakowski, F. F. Hingerl, K. V. Chudnenko, U. R. Berner, GEM-Selektor geochemical modeling package: revised algorithm and GEMS3K numerical kernel for coupled simulation codes, Computational Geosciences 17 (1) (2013) 1–24, https://doi.org/10.1007/s10596-012-9310-6.

[19] J. J. Zheng, H. S. Wong, N. R. Buenfeld, Assessing the influence of itz on the steady-state chloride diffusivity of concrete using a numerical model, Cement and Concrete Research 39 (9) (2009) 805–813, https://doi.org/10.1016/j.cemconres.2009.06.002.

[20] E. J. Garboczi, D. P. Bentz, Analytical formulas for interfacial transition zone properties, Advanced Cement Based Materials 6 (3-4) (1997) 99–108, https://doi.org/10.1016/S1065-7355(97)90016-X.

[21] K. L. Scrivener, K. M. Nemati, The percolation of pore space in the cement paste/aggregate interfacial zone of concrete, Cement and Concrete Research 26 (1) (1996) 35–40, https://doi.org/10.1016/0008-8846(95)00185-9.

[22] M. P. Lutz, R. W. Zimmerman, Effect of an inhomogeneous interphase zone on the bulk modulus and conductivity of a particulate composite, International Journal of Solids and Structures 42 (2) (2005) 429–437, https://doi.org/10.1016/j.ijsolstr.2004.06.046.

[23] Z. Hashin, P. J. M. Monteiro, An inverse method to determine the elastic properties of the interphase between the aggregate and the cement paste, Cement and Concrete Research 32 (8) (2002) 1291–1300, https://doi.org/10.1016/S0008-8846(02)00792-5.

[24] S. Caré, E. Hervé, Application of a n-phase model to the diffusion coefficient of chloride in mortar, Transport in Porous Media 56 (2) (2004) 119–135, https://doi.org/10.1023/B:TIPM.0000021730.34756.40.

[25] Z. Sun, E. J. Garboczi, S. P. Shah, Modeling the elastic properties of concrete composites: Experiment, differential effective medium theory, and numerical simulation, Cement and Concrete Composites 29 (1) (2007) 22–38, https://doi.org/10.1016/j.cemconcomp.2006.07.020.

[26] E. Stora, B. Bary, Q.-C. He, E. Deville, P. Montarnal, Modelling and simulations of the chemo–mechanical behaviour of leached cement-based materials: Leaching process and induced loss of stiffness, Cement and Concrete Research 39 (9) (2009) 763–772, https://doi.org/10.1016/j.cemconres.2009.05.010.

[27] B. Bary, S. Béjaoui, Assessment of diffusive and mechanical properties of hardened cement pastes using a multi-coated sphere assemblage model, Cement and Concrete Research 36 (2) (2006) 245–258, https://doi.org/10.1016/j.cemconres.2005.07.007.

[28] A. Hershey, The elasticity of an isotropic aggregate of anisotropic cubic crystals, Journal of Applied Mechanics-transactions of the ASME 21 (3) (1954) 236–240.

[29] E. Kröner, Bounds for effective elastic moduli of disordered materials, Journal of the Mechanics and Physics of Solids 25 (2) (1977) 137–155, https://doi.org/10.1016/0022-5096(77)90009-6.

[30] T. Mori, K. Tanaka, Average stress in matrix and average elastic energy of materials with misfitting inclusions, Acta Metallurgica 21 (5) (1973) 571–574, https://doi.org/10.1016/0001-6160(73)90064-3.

[31] D. A. G. Bruggeman, Berechnung verschiedener physikalischer konstanten von heterogenen substanzen. i. dielektrizitätskonstanten und leitfähigkeiten der mischkörper aus isotropen substanzen, Annalen der physik 416 (7) (1935) 636–664, https://doi.org/10.1002/andp.19354160705.

[32] E. Herve, A. Zaoui, n-Layered inclusion-based micromechanical modelling, International Journal of Engineering Science 31 (1) (1993) 1–10, https://doi.org/10.1016/0020-7225(93)90059-4.

[33] H. L. Duan, X. Yi, Z. P. Huang, J. Wang, A unified scheme for prediction of effective moduli of multiphase composites with interface effects: Part II—Application and scaling laws, Mechanics of Materials 39 (1) (2007) 94–103, https://doi.org/10.1016/j.mechmat.2006.02.010.

[34] F. Bernard, S. Kamali-Bernard, Numerical study of ITZ contribution on mechanical behavior and diffusivity of mortars, Computational Materials Science 102 (2015) 250–257, https://doi.org/10.1016/j.commatsci.2015.02.016.

[35] B. Bary, C. Bourcier, T. Helfer, Analytical and 3D numerical analysis of the thermoviscoelastic behavior of concrete-like materials including interfaces, Advances in Engineering Software 112 (2017) 16–30, https://doi.org/10.1016/j.advengsoft.2017.06.006.

[36] A. Idiart, J. Bisschop, A. Caballero, P. Lura, A numerical and experimental study of aggregate-induced shrinkage cracking in cementitious composites, Cement and Concrete Research 42 (2) (2012) 272–281, https://doi.org/10.1016/j.cemconres.2011.09.013.

[37] T. Wu, X.-Z. You, P. Bouř, Applications of chiroptical spectroscopy to coordination compounds, Coordination Chemistry Reviews 284 (2015) 1–18, https://doi.org/10.1016/j.ccr.2014.09.012.

[38] R. Snellings, A. Machner, G. Bolte, H. Kamyab, P. Durdzinski, P. Teck, M. Zajac, A. Muller, K. de Weerdt, M. B. Haha, Hydration kinetics of ternary slag-limestone cements: Impact of water to binder ratio and curing temperature, Cement and Concrete Research 151 (2022) 106647, https://doi.org/10.1016/j.cemconres.2021.106647.

[39] B. Lothenbach, D. A. Kulik, T. Matschei, M. Balonis, L. Baquerizo, B. Dilnesa, G. D. Miron, R. J. Myers, Cemdata18: A chemical thermodynamic database for hydrated Portland cements and alkali-activated materials, Cement and Concrete Research 115 (2019) 472–506, https://doi.org/10.1016/j.cemconres.2018.04.018.

[40] C. W. Hargis, B. Lothenbach, C. J. Müller, F. Winnefeld, Carbonation of calcium sulfoaluminate mortars, Cement and Concrete Composites 80 (2017) 123–134, https://doi.org/10.1016/j.cemconcomp.2017.03.003.

[41] Z. Shi, B. Lothenbach, M. R. Geiker, J. Kaufmann, A. Leemann, S. Ferreiro, J. Skibsted, Experimental studies and thermodynamic modeling of the carbonation of Portland cement, metakaolin and limestone mortars, Cement and Concrete Research 88 (2016) 60–72, https://doi.org/10.1016/j.cemconres.2016.06.006.

[42] A. Machner, M. Zajac, M. B. Haha, K. O. Kjellsen, M. R. Geiker, K. De Weerdt, Stability of the hydrate phase assemblage in Portland composite cements containing dolomite and metakaolin after leaching, carbonation, and chloride exposure, Cement and Concrete Composites 89 (2018) 89–106, https://doi.org/10.1016/j.cemconcomp.2018.02.013.

[43] V. Shah, K. Scrivener, B. Bhattacharjee, S. Bishnoi, Changes in microstructure characteristics of cement paste on carbonation, Cement and Concrete Research 109 (2018) 184–197, https://doi.org/10.1016/j.cemconres.2018.04.016.

[44] R. Loser, B. Lothenbach, A. Leemann, M. Tuchschmid, Chloride resistance of concrete and its binding capacity – Comparison between experimental results and thermodynamic modeling, Cement and Concrete Composites 32 (1) (2010) 34–42, https://doi.org/10.1016/j.cemconcomp.2009.08.001.

[45] C. Roosz, S. Gaboreau, S. Grangeon, D. Prêt, V. Montouillout, N. Maubec, S. Ory, P. Blanc, P. Vieillard, P. Henocq, Distribution of water in synthetic calcium silicate hydrates, Langmuir 32 (27) (2016) 6794–6805, https://doi.org/10.1021/acs.langmuir.6b00878.

[46] B. Lothenbach, A. Nonat, Calcium silicate hydrates: Solid and liquid phase composition, Cement and Concrete Research 78 (2015) 57–70, https://doi.org/10.1016/j.cemconres.2015.03.019.

[47] D. A. Kulik, Improving the structural consistency of CSH solid solution thermodynamic models, Cement and Concrete Research 41 (5) (2011) 477–495, https://doi.org/10.1016/j.cemconres.2011.01.012.

[48] B. Bary, N. Leterrier, E. Deville, P. Le Bescop, Coupled chemo-transport-mechanical modelling and numerical simulation of external sulfate attack in mortar, Cement and Concrete Composites 49 (2014) 70–83, https://doi.org/10.1016/j.cemconcomp.2013.12.010.

[49] Z. Zhu, W. Xu, H. Chen, The fraction of overlapping interphase around 2D and 3D polydisperse non-spherical particles: Theoretical and numerical models, Computer Methods in Applied Mechanics and Engineering 345 (2019) 728–747, https://doi.org/10.1016/j.cma.2018.11.022.

[50] W. Xu, H. Ma, S. Ji, H. Chen, Analytical effective elastic properties of particulate composites with soft interfaces around anisotropic particles, Composites Science and Technology 129 (2016) 10–18, https://doi.org/10.1016/j.compscitech.2016.04.011.

[51] W. Xu, Y. Wu, X. Gou, Effective elastic moduli of nonspherical particle-reinforced composites with inhomogeneous interphase considering graded evolutions of elastic modulus and porosity, Computer Methods in Applied Mechanics and Engineering 350 (2019) 535–553, https://doi.org/10.1016/j.cma.2019.03.021.

[52] W. Xu, D. Zhang, P. Lan, Y. Jiao, Multiple-inclusion model for the transport properties of porous composites considering coupled effects of pores and interphase around spheroidal particles, International Journal of Mechanical Sciences 150 (2019) 610–616, https://doi.org/10.1016/j.ijmecsci.2018.10.063.

[53] E. Stora, Q.-C. He, B. Bary, Influence of inclusion shapes on the effective linear elastic properties of hardened cement pastes, Cement and Concrete Research 36 (7) (2006) 1330–1344, https://doi.org/10.1016/j.cemconres.2006.02.007.

[54] P. P. Castañeda, J. R. Willis, The effect of spatial distribution on the effective behavior of composite materials and cracked media, Journal of the Mechanics and Physics of Solids 43 (12) (1995) 1919–1951, https://doi.org/10.1016/0022-5096(95)00058-Q.

[55] C. Liu, D. Xie, W. She, Z. Liu, G. Liu, L. Yang, Y. Zhang, Numerical modelling of elastic modulus and diffusion coefficient of concrete as a three-phase composite material, Construction and Building Materials 189 (2018) 1251–1263, https://doi.org/10.1016/j.conbuildmat.2018.08.191.

[56] C. Zhou, K. Li, F. Ma, Numerical and statistical analysis of elastic modulus of concrete as a three-phase heterogeneous composite, Computers & Structures 139 (2014) 33–42, https://doi.org/10.1016/j.compstruc.2014.04.007.

[57] F. H. Heukamp, Chemomechanics of calcium leaching of cement-based materials at different scales: The role of CH-dissolution and CSH degradation on strength and durability performance of materials and structures, Ph.D. thesis, Massachusetts Institute of Technology (2003).

[58] P. J. M. Monteiro, C. P. Ostertag, Analysis of the aggregate-cement paste interface using grazing incidence X-ray scattering, Cement and Concrete Research 19 (6) (1989) 987–988.

[59] S. Caré, Influence of aggregates on chloride diffusion coefficient into mortar, Cement and Concrete Research 33 (7) (2003) 1021–1028, https://doi.org/10.1016/S0008-8846(03)00009-7.

[60] J. Lin, Q. Zhao, H. Chen, Z. Zhu, M. Li, D. Zhao, Insight into the diffusivity of particulate composites considering percolation of soft interphases around hard fillers: From spherical to polyhedral particles, Powder Technology 392 (2021) 459–472, https://doi.org/10.1016/j.powtec.2021.06.047.

[61] Z. Pan, D. Wang, R. Ma, A. Chen, A study on ITZ percolation threshold in mortar with ellipsoidal aggregate particles, Computers and Concrete 22 (6) (2018) 551–561, https://doi.org/10.12989/cac.2018.22.6.551.

[62] J.-J. Zheng, X.-Z. Zhou, Effective medium method for predicting the chloride diffusivity in concrete with ITZ percolation effect, Construction and Building Materials 47 (2013) 1093–1098, https://doi.org/10.1016/j.conbuildmat.2013.05.108.

[63] J. Lin, H. Chen, L. Liu, Impact of polydispersity of particle shape and size on percolation threshold of 3D particulate media composed of penetrable superellipsoids, Powder Technology 360 (2020) 944–955, https://doi.org/10.1016/j.powtec.2019.10.054.

[64] J. Lin, H. Chen, Q. Zhao, M. Li, Statistical analysis of the critical percolation of ITZ around polygonal aggregates in three-phase concrete materials, Physica A: Statistical Mechanics and its Applications 572 (2021) 125878, https://doi.org/10.1016/j.physa.2021.125878.

[65] Y. Gao, G. De Schutter, G. Ye, H. Huang, Z. Tan, K. Wu, Characterization of ITZ in ternary blended cementitious composites: Experiment and simulation, Construction and Building Materials 41 (2013) 742–750, https://doi.org/10.1016/j.conbuildmat.2012.12.051.

[66] D. Lide, 1998. CRC Handbook of chemistry and physics, 78th edit, CRC Press 6 (4) (1997) 6–5.

[67] E. J. Garboczi, D. P. Bentz, Computer simulation of the diffusivity of cement-based materials, Journal of Materials Science 27 (8) (1992) 2083–2092, https://doi.org/10.1007/BF01117921.

[68] C. J. Haecker, E. J. Garboczi, J. W. Bullard, R. B. Bohn, Z. Sun, S. P. Shah, T. Voigt, Modeling the linear elastic properties of Portland cement paste, Cement and Concrete Research 35 (10) (2005) 1948–1960, https://doi.org/10.1016/j.cemconres.2005.05.001.

[69] J. Moon, S. Yoon, R. M. Wentzcovitch, P. J. M. Monteiro, First-principles elasticity of monocarboaluminate hydrates, American Mineralogist 99 (7) (2014) 1360–1368, https://doi.org/10.2138/am.2014.4597.

[70] B. O'Neill, J. D. Bass, G. R. Rossman, Elastic properties of hydrogrossular garnet and implications for water in the upper mantle, Journal of Geophysical Research: Solid Earth 98 (B11) (1993) 20031–20037, https://doi.org/10.1029/93JB02005.

[71] M. Zajac, J. Skocek, S. Adu-Amankwah, L. Black, M. B. Haha, Impact of microstructure on the performance of composite cements: Why higher total porosity can result in higher strength, Cement and Concrete Composites 90 (2018) 178–192, https://doi.org/10.1016/j.cemconcomp.2018.03.023.

[72] K. Velez, S. Maximilien, D. Damidot, G. Fantozzi, F. Sorrentino, Determination by nanoindentation of elastic modulus and hardness of pure constituents of Portland cement clinker, Cement and Concrete Research 31 (4) (2001) 555–561, https://doi.org/10.1016/S0008-8846(00)00505-6.

[73] J. Němeček, V. Šmilauer, L. Kopecký, Nanoindentation characteristics of alkali-activated aluminosilicate materials, Cement and Concrete Composites 33 (2) (2011) 163–170, https://doi.org/10.1016/j.cemconcomp.2010.10.005.

[74] P. Termkhajornkit, Q. H. Vu, R. Barbarulo, S. Daronnat, G. Chanvillard, Dependence of compressive strength on phase assemblage in cement pastes: Beyond gel–space ratio – Experimental evidence and micromechanical modeling, Cement and Concrete Research 56 (2014) 1–11, https://doi.org/10.1016/j.cemconres.2013.10.007.

[75] T. Honorio, L. Brochard, B. Bary, Statistical variability of mechanical fields in thermo-poro-elasticity: Multiscale analytical estimations applied to cement-based materials at early-age, Cement and Concrete Research 110 (2018) 24–41, https://doi.org/10.1016/j.cemconres.2018.05.010.

[76] O. Bernard, F.-J. Ulm, E. Lemarchand, A multiscale micromechanics-hydration model for the early-age elastic properties of cement-based materials, Cement and Concrete Research 33 (9) (2003) 1293–1309, https://doi.org/10.1016/S0008-8846(03)00039-5.

[77] G. De Schutter, L. Taerwe, Degree of hydration-based description of mechanical properties of early age concrete, Materials and Structures 29 (6) (1996) 335–344, https://doi.org/10.1007/BF02486341.

[78] V. Šmilauer, Z. Bittnar, Microstructure-based micromechanical prediction of elastic properties in hydrating cement paste, Cement and Concrete Research 36 (9) (2006) 1708–1718, https://doi.org/10.1016/j.cemconres.2006.05.014.

[79] B. Bary, M. B. Haha, E. Adam, P. Montarnal, Numerical and analytical effective elastic properties of degraded cement pastes, Cement and Concrete Research 39 (10) (2009) 902–912, https://doi.org/10.1016/j.cemconres.2009.06.012.

[80] E. 843-2, Advanced technical ceramics - mechanical properties of monolithic ceramics at room temperature - Part 2: Determination of young's modulus, shear modulus and poisson's ratio, European Committee for Standardization, Brussels (2006) .

[81] N. Bunke, Prüfung von beton. empfehlungen und hinweise als ergänzung zu din 1048, Deutscher Ausschuss für Stahlbeton (1991) 442.

[82] S.-H. Han, J.-K. Kim, Effect of temperature and age on the relationship between dynamic and static elastic modulus of concrete, Cement and Concrete Research 34 (7) (2004) 1219–1227, https://doi.org/10.1016/j.cemconres.2003.12.011.

[83] K. A. MacDonald, D. O. Northwood, Experimental measurements of chloride ion diffusion rates using a two-compartment diffusion cell: Effects of material and test variables, Cement and Concrete Research 25 (7) (1995) 1407–1416, https://doi.org/10.1016/0008-8846(95)00135-Y.

[84] F. Bernard, S. Kamali-Bernard, Predicting the evolution of mechanical and diffusivity properties of cement pastes and mortars for various hydration degrees – A numerical simulation investigation, Computational Materials Science 61 (2012) 106–115, https://doi.org/10.1016/j.commatsci.2012.03.023.

[85] https://www.salome platform.org., Salome.

[86] www.distene.com., Distene.

[87] T. De Larrard, B. Bary, E. Adam, F. Kloss, Influence of aggregate shapes on drying and carbonation phenomena in 3D concrete numerical samples, Computational Materials Science 72 (2013) 1–14, https://doi.org/10.1016/j.commatsci.2013.01.039.

[88] www cast3m.cea.fr., Cast3m.

[89] C. M. Neubauer, H. M. Jennings, E. J. Garboczi, A three-phase model of the elastic and shrinkage properties of mortar, Advanced Cement Based Materials 4 (1) (1996) 6–20, https://doi.org/10.1016/S1065-7355(96)90058-9.

[90] C.-C. Yang, J. K. Su, Approximate migration coefficient of interfacial transition zone and the effect of aggregate content on the migration coefficient of mortar, Cement and Concrete Research 32 (10) (2002) 1559–1565, https://doi.org/10.1016/S0008-8846(02)00832-3.

[91] C.-C. Yang, C.-H. Liang, Determining the steady-state chloride migration coefficient of ITZ in mortar by using the accelerated chloride migration test, Journal of the Chinese Institute of Engineers 37 (7) (2014) 892–898, https://doi.org/10.1080/02533839.2014.888813.

[92] A. Leemann, P. Nygaard, J. Kaufmann, R. Loser, Relation between carbonation resistance, mix design and exposure of mortar and concrete, Cement and Concrete Composites 62 (2015) 33–43, https://doi.org/10.1016/j.cemconcomp.2015.04.020.

[93] A. Morandeau, M. Thiery, P. Dangla, Investigation of the carbonation mechanism of CH and CSH in terms of kinetics, microstructure changes and moisture properties, Cement and Concrete Research 56 (2014) 153–170, https://doi.org/10.1016/j.cemconres.2013.11.015.

[94] V. T. Ngala, C. L. Page, Effects of carbonation on pore structure and diffusional properties of hydrated cement pastes, Cement and Concrete Research 27 (7) (1997) 995–1007, https://doi.org/10.1016/S0008-8846(97)00102-6.

[95] L. De Ceukelaire, D. Van Nieuwenburg, Accelerated carbonation of a blast-furnace cement concrete, Cement and Concrete Research 23 (2) (1993) 442–452, https://doi.org/10.1016/0008-8846(93)90109-M.

[96] H. Justnes, J. Skocek, T. A. Østnor, C. J. Engelsen, O. Skjølsvold, Microstructural changes of hydrated cement blended with fly ash upon carbonation, Cement and Concrete Research 137 (2020) 106192, https://doi.org/10.1016/j.cemconres.2020.106192.

[97] A. Morandeau, M. Thiéry, P. Dangla, Impact of accelerated carbonation on OPC cement paste blended with fly ash, Cement and Concrete Research 67 (2015) 226–236, https://doi.org/10.1016/j.cemconres.2014.10.003.

[98] L. C. Lange, C. D. Hills, A. B. Poole, The effect of accelerated carbonation on the properties of cement-solidified waste forms, Waste Management 16 (8) (1996) 757–763, https://doi.org/10.1016/S0956-053X(97)00022-6.

[99] P. H. R. Borges, J. O. Costa, N. B. Milestone, C. J. Lynsdale, R. E. Streatfield, Carbonation of CH and C-S-H in composite cement pastes containing high amounts of BFS, Cement and Concrete Research 40 (2) (2010) 284–292, https://doi.org/10.1016/j.cemconres.2009.10.020.

[100] M. Auroy, S. Poyet, P. Le Bescop, J.-M. Torrenti, T. Charpentier, M. Moskura, X. Bourbon, Comparison between natural and accelerated carbonation (3% CO_2): Impact on mineralogy, microstructure, water retention and cracking, Cement and Concrete Research 109 (2018) 64–80, https://doi.org/10.1016/j.cemconres.2018.04.012.

[101] K. Wan, Q. Xu, Y. Wang, G. Pan, 3D spatial distribution of the calcium carbonate caused by carbonation of cement paste, Cement and Concrete Composites 45 (2014) 255–263, https://doi.org/10.1016/j.cemconcomp.2013.10.011.

[102] J. Marchand, D. P. Bentz, E. Samson, Y. Maltais, Influence of calcium hydroxide dissolution on the transport properties of hydrated cement systems, Reactions of calcium hydroxide in concrete. Westerville, OH: American Ceramic Society (2001) 113–129.

Appendix A. Generalized Self Consistent Scheme

The effective bulk modulus of mortar estimated by the GSCS scheme can be expressed as:

$$k_{\text{mortar}} = k_{\text{cp}} + \frac{\phi_{\text{sand}} + \phi_{\text{ITZ}}}{\frac{1}{k_{\text{C}} - k_{\text{cp}}} + \frac{3\phi_{\text{cp}}}{3k_{\text{cp}} + 4\mu_{\text{cp}}}}; \quad \text{with } k_{\text{C}} = k_{\text{ITZ}} + \frac{\phi_{\text{sand}}}{\frac{\phi_{\text{sand}} + \phi_{\text{ITZ}}}{k_{\text{sand}} - k_{\text{ITZ}}} + \frac{\phi_{\text{ITZ}}}{3k_{\text{ITZ}} + 4\mu_{\text{ITZ}}}} \tag{A.1}$$

where ϕ_i is the volume fraction of the i-th phase, k_i and μ_i are their bulk modulus and shear modulus; cp represents the cement paste. These equations are also applicable to estimate the bulk modulus of concrete, providing that the subscripts mortar, cp and sand are replaced by concrete, mortar and aggregates. Lengthy expressions of the shear modulus obtained with GSCS are not recalled here, see e.g. [32] for further details.

The diffusive properties of both mortar and concrete by the GSCS scheme are expressed as [26]:

$$D_{\text{mortar}} = 2D_{\text{cp}}\left(\frac{3}{2 + \phi_{\text{fine aggre}} - 2\phi_{\text{ITZ}}\beta_{\text{ITZ}}^{\text{cp}}} - 1\right); \quad \text{with } \beta_{\text{ITZ}}^{\text{cp}} = \frac{D_{\text{cp}} - D_{\text{ITZ}}}{D_{\text{cp}} + 2D_{\text{ITZ}}} \tag{A.2}$$

$$D_{\text{con.}} = 2D_{\text{mortar}}\left(\frac{3}{2 + \phi_{\text{coarse aggre}} - 2\phi_{\text{ITZ}}\beta_{\text{ITZ}}^{\text{mortar}}} - 1\right); \text{ with } \beta_{\text{ITZ}}^{\text{mortar}} = \frac{D_{\text{mortar}} - D_{\text{ITZ}}}{D_{\text{mortar}} + 2D_{\text{ITZ}}} \tag{A.3}$$

where D_{cp}, D_{mortar}, $D_{\text{con.}}$, D_{ITZ} are the diffusive coefficients of cement paste, mortar, concrete and ITZ, respectively; $\phi_{\text{fine aggre}}$, $\phi_{\text{coarse aggre}}$, and ϕ_{ITZ} are the volume fractions of the fine aggregate, coarse aggregate and the ITZ.

Appendix B. Replacement procedure

The bulk and shear modulus of the equivalent inclusion can be estimated as [33]:

$$k_{eq} = \frac{m_r k_i \mu_m}{3k_i + m_r \mu_m} \tag{B.1}$$

$$\mu_{eq} = \frac{\mu_i(24Mm_\theta + m_r(16M + m_\theta N))}{80g_3M + 4g_3m_\theta(10(7 - v_i) + M) + m_r(2g_3(140 - 80v_i + 3M)) + m_\theta N} \tag{B.2}$$

with $k_n = \frac{2\mu_{\mathrm{ITZ}}(1-v_{\mathrm{ITZ}})}{h(1-2v_{\mathrm{ITZ}})}$, $k_t = \frac{\mu_{\mathrm{ITZ}}}{h}$, $M = g_3(7 + 5v_i)$, $N = 5(28 - 40v_i + M)$, $g_3 = \frac{\mu_i}{\mu_m}$, $m_r = \frac{k_n R_i}{\mu_m}$, and $m_\theta = \frac{k_t R_i}{\mu_m}$. In these equations, μ_{ITZ} and v_{ITZ} are the shear modulus and the Poisson's ratio of the ITZ interphase, h is the ITZ thickness; k_i and μ_i are the bulk and shear modulus of the i-th inclusion, v_i and R_i are their Poisson's ratio and radius, $i \in$ (fine aggregate, coarse aggregate); μ_m is the shear modulus of the matrix, and $m \in$ (cement paste, mortar).

Appendix C. Additional information to section 4.1.2: Estimated Young's modulus of the mortar with w/c=0.40, 0.50, and 0.60 via various schemes

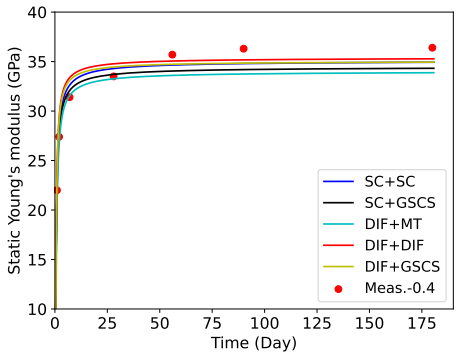

(a) Estimated Young's modulus of the mortar with w/c=0.40 via various schemes;

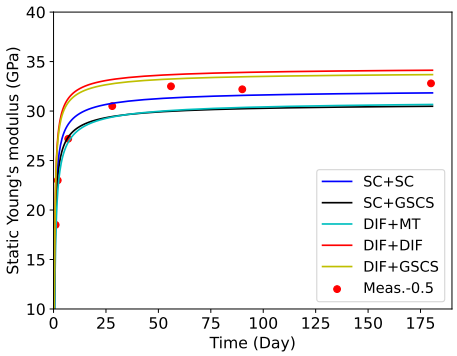

(b) Estimated Young's modulus of the mortar with w/c=0.50 via various schemes;

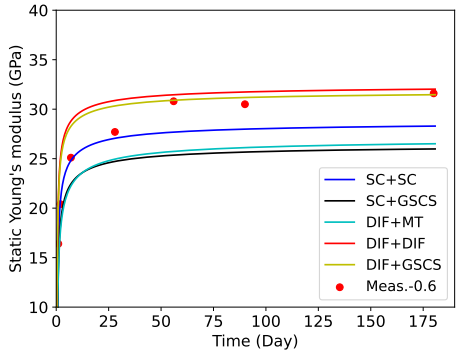

(c) Estimated Young's modulus of the mortar with w/c=0.60 via various schemes.

Figure C.23: Estimated Young's modulus of the mortar with w/c=0.40, 0.50, and 0.60 via various schemes: SC+SC, SC+GSCS, DIF+MT, DIF+DIF, and DIF+GSCS.